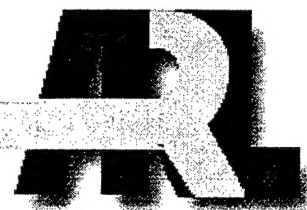ARMY RESEARCH LABORATORY

Dynamic Vivacity and Its Application to Conventional and Electrothermal-Chemical (ETC) Closed Chamber Results

William F. Oberle

ARL-TR-2631   DECEMBER 2001

20020118 014

Army Research Laboratory
Aberdeen Proving Ground, MD 21005-5066

Dynamic Vivacity and Its Application to Conventional and Electrothermal-Chemical (ETC) Closed Chamber Results

William F. Oberle
Weapons and Materials Research Directorate

Abstract

Historically, dynamic vivacity has been used extensively in propellant lot acceptance. More recently, dynamic vivacity has been used in the analysis of closed chamber experimental data to assess propellant grain surface area behavior during combustion. The objective of this report is to (a) examine the physical meaning of dynamic vivacity; (b) theoretically explore the behavior of dynamic vivacity for conventionally ignited charges of various geometries, including layered propellant charges; and (c) determine the appropriate method for applying dynamic vivacity to electrothermal-chemical (ETC) closed chamber data. The results presented indicate that dynamic vivacity is a robust statistic for assessing grain surface area behavior during combustion as long as the burn rate exponent in Vielle's Law is between approximately 0.7 and 1.0. If the burn rate exponent is greater than 1.0, the nature of the propellant surface area deduced from the dynamic vivacity appears to be distorted. In these cases, the dynamic vivacity always indicates a progressive grain geometry. From the cases studied, it appears that grain fracture during combustion will not significantly change the dynamic vivacity results unless the original grain possess a progressive grain geometry and the fractured grain pieces are relatively large. Finally, it appears that ETC ignition does not impact the shape of the dynamic vivacity curve but only affects the magnitude of the curve.

ACKNOWLEDGMENTS

INTENTIONALLY LEFT BLANK

Contents

DYNAMIC VIVACITY AND ITS APPLICATION TO CONVENTIONAL AND ELECTRO-THERMAL-CHEMICAL (ETC) CLOSED CHAMBER RESULTS

1. Introduction

Modern high performance weapon systems for both direct and indirect fire applications require highly repeatable interior ballistics in order to be effective. Although significant advances have been made in the development of robust ignition systems and charge configurations that enhance repeatability, lot-to-lot and within-lot variations in propellant properties can lead to unacceptable performance. Thus, ballisticians have developed a number of protocols that are employed for propellant acceptance. These protocols generally combine results of theoretical calculations, laboratory experiments, and controlled gun firings. An important diagnostic for laboratory experimentation involves the use of a closed vessel in which the pressure history of a burning propellant is recorded. From the pressure history, information concerning the combustion behavior of the propellant can be deduced and compared to reference propellants for lot acceptance [1, 2] or in the case of experimental propellants, the information can be used in ballistic simulations to estimate potential performance.

Dynamic vivacity is one of several statistics that can be derived from the closed vessel pressure history. According to Klingaman and Doman [3], "Several synonyms and definitions are used in the literature referring to vivacity, but not all have the same physical meaning"[1]. In this report, dynamic vivacity will be defined as in most of the references contained in [3] as

$$A(t) = \frac{dP(t)/dt}{P(t) * P_{max}}.$$ (1)

The objective of this work is to (a) examine the physical meaning of the dynamic vivacity as defined in Equation (1); (b) theoretically explore the behavior of the dynamic vivacity for conventionally ignited charges of various geometries, including layered propellant charges; and (c) determine the appropriate method for applying dynamic vivacity to electro-thermal-chemical (ETC) closed vessel data.

---

[1] In their paper, Klingaman and Doman [3] provide a detailed review of the literature about vivacity and the different uses of the term.

2. Physical Interpretation

Following the approach of Machalka [4], we can obtain an expression for the dynamic vivacity as defined in Equation (1) as follows:

$$P(t)\left[V_0 - \frac{m_0}{\rho}(1-z(t)) - bm_0 z(t)\right] = n(t)RT \tag{2}$$

The Nobel-Abel equation of state [5] extends the equation of state for an ideal gas by accounting for the volume of the gas molecules. It is commonly used in both interior ballistic gun and closed vessel calculations. Note that this equation is a simplification of the actual situation occurring in the closed chamber. The presence of air in the chamber is ignored and the gas temperature is assumed to be constant. A constant gas temperature is equivalent to assuming a uniform heat loss. Fortunately, these assumptions will not have a large impact on the calculations as long as the mass of air is small in comparison to the propellant; e.g., less than 1% to 2% and conventional ignition of the propellant is used. Letting $z(t) = 1$ in Equation (2) (i.e., all burnt condition), an expression for the maximum pressure is obtained

$$P_{max} = \frac{\left(\frac{m_0}{M}\right)RT}{V_0 - bm_0}. \tag{3}$$

Now, substituting $n(t) = m_0 z(t)/M$ for $n(t)$ in Equation (2) and solving for $z(t)$,

$$z(t) = \frac{P(t)\left[V_0 - \frac{m_0}{\rho}\right]}{\left(\frac{m_0}{M}\right)RT + P(t)\left[bm_0 - \frac{m_0}{\rho}\right]}. \tag{4}$$

Substituting Equation (3) into Equation (4),

$$z(t) = \frac{P(t)\left[V_0 - \frac{m_0}{\rho}\right]}{P_{max}\left[V_0 - bm_0\right] + P(t)\left[bm_0 - \frac{m_0}{\rho}\right]}. \tag{5}$$

Dividing numerator and denominator by $P(t)$ and V_0, and letting $d = m_0/V_0$, the initial propellant loading density, Equation (5) can be rewritten as

$$z(t) = \frac{\left[1 - \frac{d}{\rho}\right]}{\frac{P_{max}}{P(t)}\left[1 - bd\right] + \left[bd - \frac{d}{\rho}\right]}. \tag{6}$$

2

Differentiating with respect to t,

$$\frac{dz(t)}{dt} = \frac{P_{max} \, dP(t)/dt}{P^2(t)} \frac{\left[1 - d/\rho\right]\left[1 - bd\right]}{\left[\frac{P_{max}}{P(t)}(1 - bd) + \left(bd - d/\rho\right)\right]^2}, \tag{7}$$

or,

$$\frac{dz(t)}{dt} = \frac{dP(t)/dt}{P_{max}} \frac{\left[1 - d/\rho\right]\left[1 - bd\right]}{\left[(1 - bd) + \frac{P(t)}{P_{max}}\left(bd - d/\rho\right)\right]^2}. \tag{8}$$

Next, a second expression for the time derivative of $z(t)$ is developed. By definition, the propellant burn rate is given by

$$r(t) = \frac{m_0 \frac{dz(t)}{dt}}{\rho S(t)}. \tag{9}$$

Thus,

$$\frac{dz(t)}{dt} = \frac{r(t)\rho S(t)}{m_0} = \frac{r(t)S(t)}{V_p}. \tag{10}$$

Equating Equations (8) and (10),

$$\frac{r(t)S(t)}{V_p} = \frac{dP(t)/dt}{P_{max}} \frac{\left[1 - d/\rho\right]\left[1 - bd\right]}{\left[(1 - bd) + \frac{P(t)}{P_{max}}\left(bd - d/\rho\right)\right]^2}. \tag{11}$$

Solving for the dynamic vivacity,

$$A(t) = \frac{dP(t)/dt}{P(t) * P_{max}} = \frac{r(t)S(t)}{V_p P(t)} \frac{\left[(1 - bd) + \frac{P(t)}{P_{max}}\left(bd - d/\rho\right)\right]^2}{\left[1 - d/\rho\right]\left[1 - bd\right]}. \tag{12}$$

As can be observed in Equation (12), the dynamic vivacity depends on the instantaneous propellant burn rate, $r(t)$, propellant surface area, $S(t)$, chamber pressure, $P(t)$, maximum chamber pressure, P_{max}, propellant chamber loading density, d, and two propellant physical properties, covolume, b, and density, ρ. Thus, dynamic vivacity has no direct correlation to a single propellant property. As Klingaman and Domen [3] state, "...[vivacity] is sensitive to the propellant composition and actual propellant surface area." The sensitivity to surface area is clear. The sensitivity to propellant composition is through the burn rate, covolume, and density. Finally, since $P(t)$ is generally a

3

monotonically increasing function of t, dynamic vivacity is often expressed as a function of $P(t)/P_{max}$.

3. Dynamic Vivacity and Propellant Surface Area

Propellants are classified as having a progressive, neutral, or regressive[2] geometry, depending on whether the surface area increases, remains the same, or decreases as the depth into the grain increases, i.e., the slope of the surface area curve is positive, effectively zero, or negative. These concepts are illustrated in Figure 1 for several grain geometries. As indicated in Equation (9), knowledge of the instantaneous propellant surface area is critical for determining propellant burn rate. Unfortunately, there is no direct experimental method for measuring the surface area of a burning propellant grain. In general, surface area information is gathered by deduction. One approach is to assume knowledge of the propellant burn rate and then use the closed chamber pressure together with the burn rate to calculate the surface area. This is useful when one is handling known propellants when grain fracture is suspected. However, this does not work with experimental propellants when the burn rate is to be determined. Historically, the dynamic vivacity has been used to assess the propellant geometric progressivity and whether the propellant surface area was suffering any fracture.
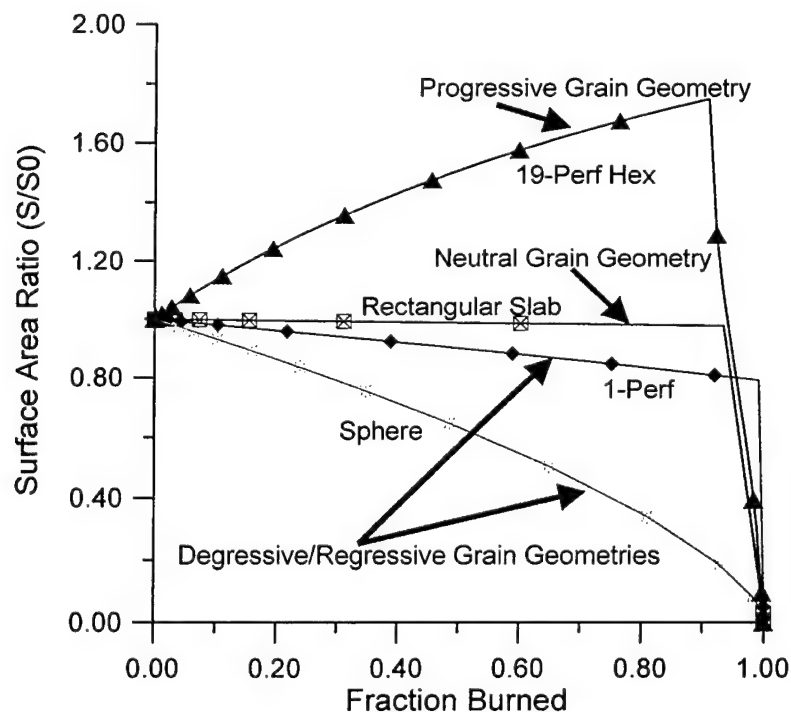
Figure 1. Surface Area Ratios for Various Grain Geometries.

---

[2]Also referred to as "degressive."

To explore this use of the dynamic vivacity, consider the time derivative of the dynamic vivacity,

$$
\frac{dA(t)}{dt} = \frac{\left[(1-bd)+\dfrac{P(t)}{P_{max}}\left(bd-\dfrac{d}{\rho}\right)\right]^2}{\left[1-\dfrac{d}{\rho}\right]\left[1-bd\right]}\left(\frac{\dot{r}(t)S(t)}{V_p P(t)}+\frac{r(t)\dot{S}(t)}{V_p P(t)}-\frac{r(t)S(t)\dot{P}(t)}{V_p P^2(t)}\right)+
$$

$$
\frac{2r(t)S(t)\dot{P}(t)}{V_p P(t)P_{max}}\frac{\left[(1-bd)+\dfrac{P(t)}{P_{max}}\left(bd-\dfrac{d}{\rho}\right)\right]\left[bd-\dfrac{d}{\rho}\right]}{\left[1-\dfrac{d}{\rho}\right]\left[1-bd\right]},
$$

(13)

in which the dot notation represents a time derivative. From Equation (13), it is not clear that the sign of the derivative of the dynamic vivacity and surface area will be the same, i.e., the slope of the dynamic vivacity will mirror the slope of the surface area curve. To further investigate the relationship of vivacity to surface area expressed in Equation (13), the behavior of the three expressions in (14) must be investigated.

$$
1-\frac{d}{\rho}, \qquad 1-bd, \qquad bd-\frac{d}{\rho}
$$

(14)

Since the maximum loading density, d, is the propellant density, ρ, the first expression will always be non-negative. In fact, it will be strictly positive since having the chamber totally filled with propellant is a nearly physically impossible situation. Figure 2 shows the behavior of the second expression, $1 - bd$, for various values of propellant covolume and loading density. Typical closed chamber loading densities, d, are generally between 100 kg/m³ and 350 kg/m³. For most propellants, the covolume is approximately 10^{-3} m³/kg. Thus, the shaded box in Figure 2 represents the range of covolume and loading density typical of closed chamber operations. As can be observed in Figure 2, $1 - bd$ is positive in this region. In fact, over a wide range for the propellant covolume, this term remains positive unless the loading density increases dramatically.

However, as indicated in Figure 3, the closed chamber pressure increases to extremely high pressures (5+ GPa) as the loading density approaches values (800 kg/m³) necessary to make the expression $1 - bd$ negative. The graph in Figure 3 is based on the propellant JA2. From a physical standpoint, $1 - bd$ cannot be negative. This expression is equivalent to

$$
\frac{1}{V_0}(V_0 - bm_0).
$$

(15)
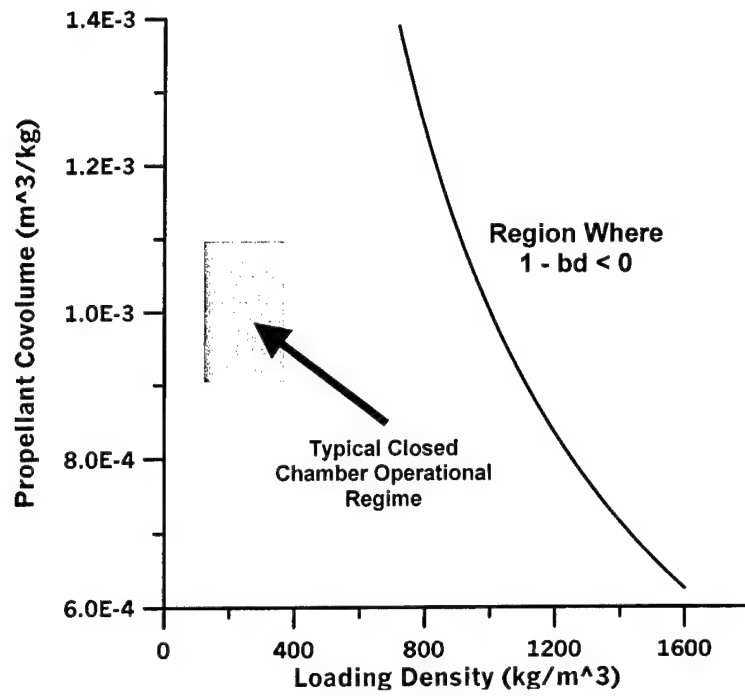
Figure 2. Behavior of the Constant 1 - bd.
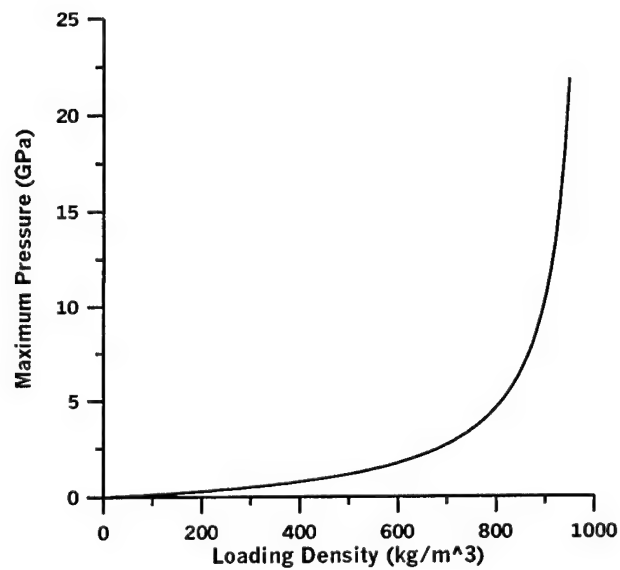
Figure 3. Pressure Versus Loading Density for a Closed Chamber.
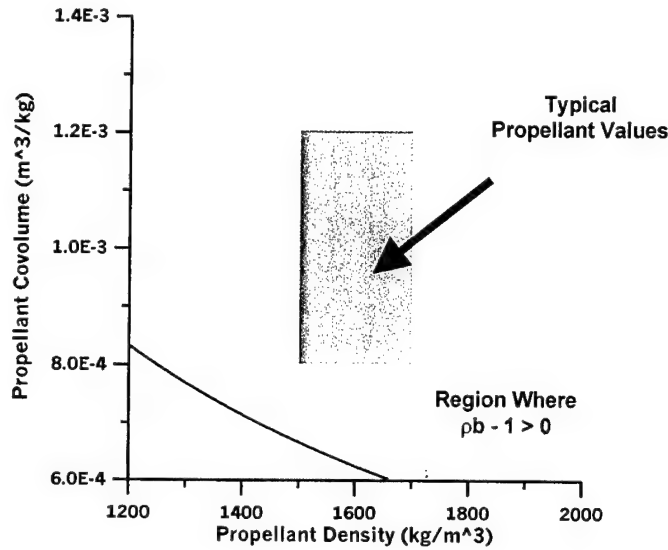
Figure 4. Behavior of pb - 1.

If it is negative, that would mean that the volume of the gas molecules (bm_0) would exceed the volume of the closed chamber, V_0. This leaves the last expression that can be rewritten as

$$\frac{d}{\rho}(\rho b - 1).\tag{16}$$

Figure 4 is similar to Figure 2 and indicates that for a wide range of values of propellant density and covolume, the expression in (16) will be positive. Note that this expression depends solely on propellant properties and not on the closed chamber configuration. Thus, for any realistic closed chamber experiment, the three expressions in (14) will be positive.

Assuming that the propellant burn rate and pressure history for the closed chamber are strictly increasing, their derivatives will be positive. Therefore, the second term of Equation (13) will always be positive and the sign of the first term will depend on the sign of the expression

$$\frac{\dot{r}(t)S(t)}{V_p P(t)} + \frac{r(t)\dot{S}(t)}{V_p P(t)} - \frac{r(t)S(t)\dot{P}(t)}{V_p P^2(t)}.\tag{17}$$

Assuming that Vielle's Law,

$$r(t) = \beta P^\alpha(t),\tag{18}$$

accurately describes the propellant burn rate, the expression in (17) becomes

$$\frac{r(t)}{V_p P(t)} \left(\frac{\dot{P}(t)}{P(t)} S(t)(\alpha - 1) + \dot{S}(t) \right). \tag{19}$$

For progressive grain geometries, if α is ≥ 1, then the expression in (19) will always be positive since dS/dt is positive for progressive grains. Thus, Equation (13) will be positive, and dA/dt and dS/dt will have the same sign. On the other hand, even for progressive grain geometries, if α is <1, the expression in (19) could be negative and it is possible that Equation (13) could also be negative. Thus, the dynamic vivacity need not always track with surface area, i.e., the slope of the dynamic vivacity may be negative while the slope of the surface area curve is positive.

To illustrate, consider Figures 5 and 6 that show the results of a simulated closed chamber experiment for a cylindrical grain geometry with 19 perforations (19-perf). For the simulation, the propellant loading density is 300 kg/m³ (0.3 g/cm³) and the propellant formulation is essentially that of JA2. The simulation is performed with the interior ballistics code IBHVG2 [6] with a sufficiently large shot start pressure so that no projectile motion occurs (i.e., a closed chamber).

Figure 5 gives the surface area ratio (instantaneous surface area/initial surface area) as a function of P/P_{max}. As expected, the 19-perf cylindrical grain geometry is progressive to about 80% of maximum pressure at which time, the web is burned through, the grain slivers, and the grain geometry becomes regressive. Although the surface area ratio is generally graphed as a function of propellant mass fraction burned (see Figure 1), virtually the same curve will result when the surface area ratio is plotted as a function of P/P_{max}. Therefore, for ease in comparing surface area ratio graphs and dynamic vivacity graphs, the surface area ratio will be plotted versus P/P_{max} in this report.

Figure 6 gives the dynamic vivacity for the simulation and clearly shows (to about 20% of maximum pressure) that the dynamic vivacity can have a negative slope while the surface area has a positive slope[3]. However, from 20% of maximum pressure to the point of slivering (~80% maximum pressure), the dynamic vivacity does have a positive slope, consistent with the progressive grain geometry. For the simulation, the burn rate exponent is 0.844. If the simulation is re-done with a burn rate of 1.1, as discussed before, the slope of the dynamic vivacity and surface area would be expected to be the same. The expected result is shown in Figure 7. In either case, if the dynamic vivacity curve is being used to deduce grain geometry, one would conclude a progressive grain geometry. The negative slope at the start of the dynamic vivacity curve when the burn rate exponent is 0.844 would most likely be ignored and attributed to variability in

---

[3]As noted by Dr. Barrie Homan in his review, this effect is likely a result of the impact that a low value of pressure has on Equation (13). As Dr. Homan showed, the value of Equation (13) is proportional to (C $*P(t)/P_{max}$+ $(\alpha$-1) + dS(t)/dt$*P(t)/(S(t)*dP(t)/dt))$ in which C is a constant less than 0.8 for practical closed chamber conditions. For small values of $P(t)$, this expression can be negative. For example, if $P(t)/P_{max}$ is approximately 0.1, the first term would be on the order of 0.08 and the last term could also be small since the pressure derivative is generally large. Thus, their sum could be less than 0.1 to 0.15, which would be typical values for $-(\alpha$-1).

propellant ignition and flame spread, which is discussed in a later section. An examination of Figures 6 and 7 does indicate a strong dependence of dA/dt or equivalently, $dA/d(P/P_{max})$, i.e., slope of dynamic vivacity curve, on the burn rate exponent. In Figure 6, the curve rises from approximately 0.8 to 1.0. For the higher burn rate exponent, the dynamic vivacity curve rises from approximately 2.5 to 5 over the same range of values of P/P_{max} (0.2 to 0.8). To further explore this dependence on the burn rate exponent, simulated dynamic vivacity curves for the 19-perf cylindrical grain geometry are computed for burn rate exponents of 0.4 (Figure 8) and 1.3 (Figure 9). As can be observed in Figure 8, as the burn rate exponent decreases, the dynamic vivacity curve approaches that expected for a neutral grain geometry. Figure 9 indicates that as the burn rate increases, the slope of the dynamic vivacity also increases.
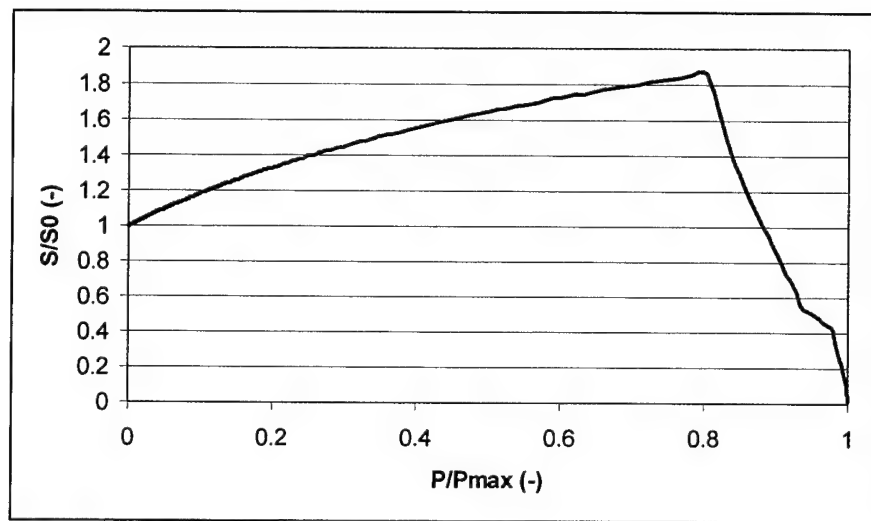

Figure 5. Surface Area Ratio for 19-perf Cylindrical Grain Geometry.

Figure 6. Dynamic Vivacity for 19-perf Cylindrical Grain Geometry With a Burn Rate Exponent of 0.844.

Figure 7. Dynamic Vivacity for 19-perf Cylindrical Grain Geometry With a Burn Rate Exponent of 1.1.
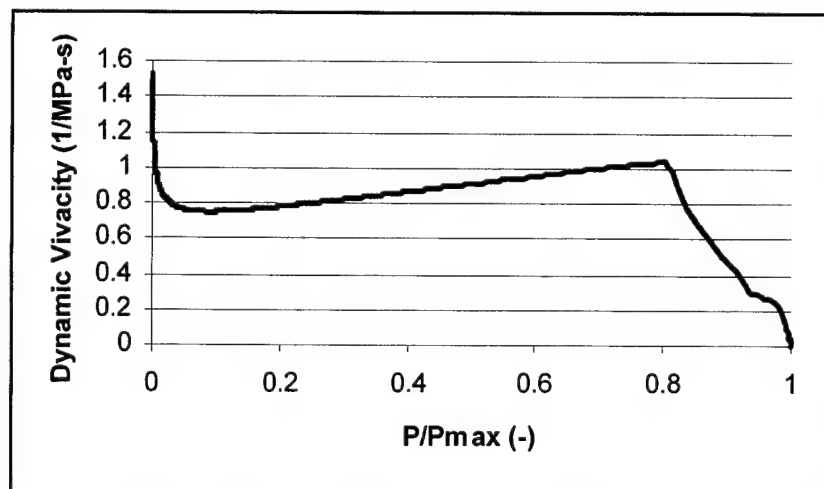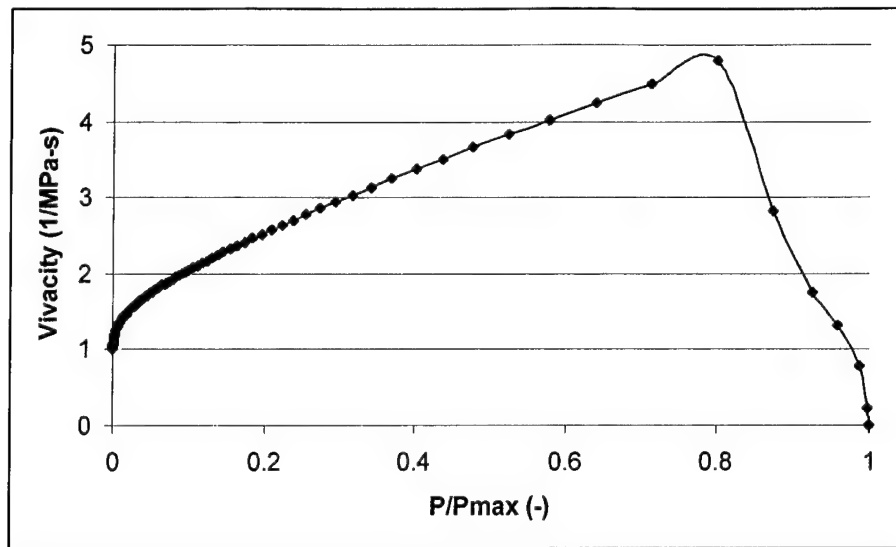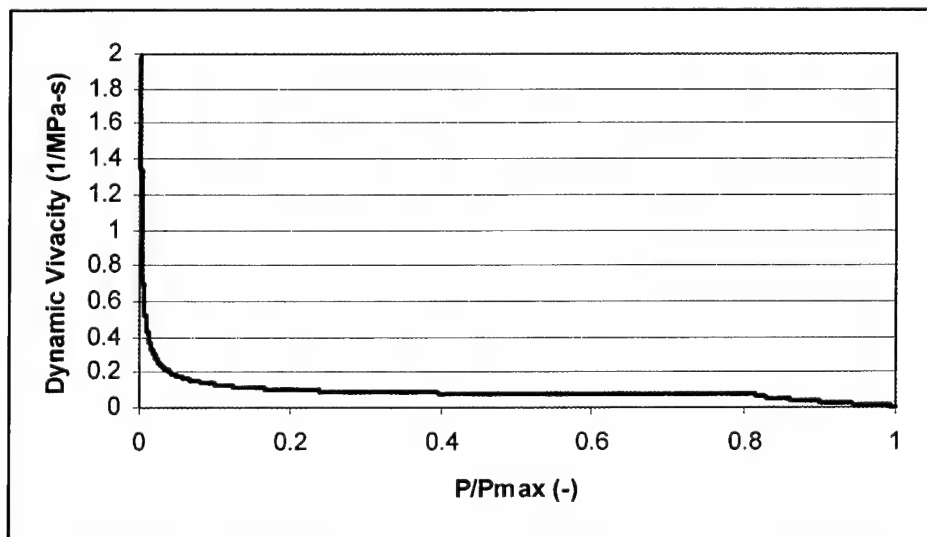

Figure 8. Dynamic Vivacity for 19-perf Cylindrical Grain Geometry With a Burn Rate Exponent of 0.4.
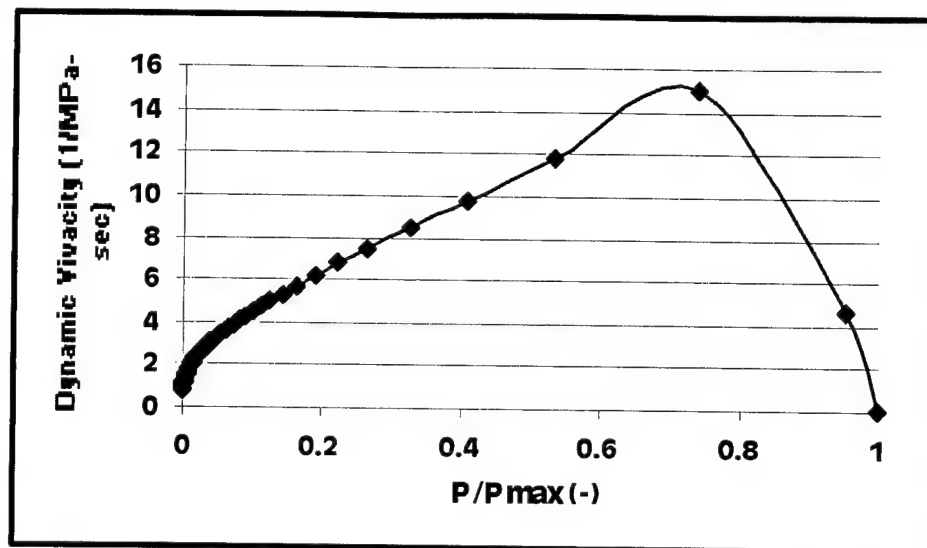
Figure 9. Dynamic Vivacity for 19-perf Cylindrical Grain Geometry With a Burn Rate Exponent of 1.3.

To determine the relationship between the dynamic vivacity and grain surface area, neutral and regressive grain geometries must be investigated. Figures 10, 11, 12, and 13 show the results of a similar analysis to the one for the progressive grain geometry. For the simulations, the propellant parameters (except for the grain geometry) remain the same. A rectangular slab geometry is used for the neutral grain geometry and a spherical geometry is used for the regressive grain geometry. Figures 10 and 12 give the surface area ratio curves, and Figures 11 and 13 show the dynamic vivacity plots for the different burn rate exponents. The neutral grain geometry of the rectangular slab geometry is clearly evident in Figure 10. As shown in Figure 11, the dynamic vivacity varies as a function of the burn rate exponent, indicating a neutral grain geometry at the lower burn rate exponents to a progressive grain geometry as the burn rate exponent increases above 1. For a neutral grain geometry $dS/dt = 0$; thus, from the expression in (19) and Equation (13), if the burn rate exponent is ≥ 1 and the grain geometry is neutral, the first term of Equation (13) is positive and dA/dt ($dA/d[P/P_{max}]$) will always be positive, indicating a progressive grain geometry. From the experimental viewpoint, using a neutral grain geometry in the closed chamber experiment provides an indication of the burn rate exponent. Assuming no grain fracture or in-depth burning, which is not unreasonable for grain geometries such as rectangular slabs, if the dynamic vivacity curve has a positive slope, then the burn rate exponent is most likely greater than 1.

The regressive nature of the spherical grain geometry is illustrated in Figure 12. Figure 13 shows the dynamic vivacity simulation results for different values of the propellant burn rate exponent. Surprisingly, the dynamic vivacity curves appear to be similar to the dynamic vivacity curves for the neutral grain geometry shown in Figure 11, except for the case when the burn rate exponent is 0.844. In this case, the dynamic vivacity reflects the regressive nature of the spherical grain geometry. The

11

major difference for the other curves is in the magnitude of the dynamic vivacity for the cases in which the burn rate exponent is >1.
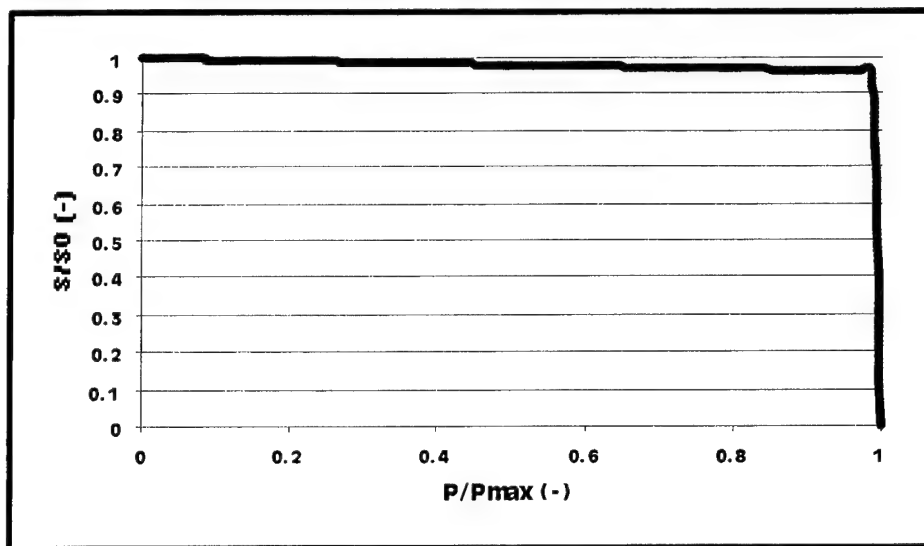
Figure 10. Surface Area Ratio for Rectangular Slab (neutral) Grain Geometry.
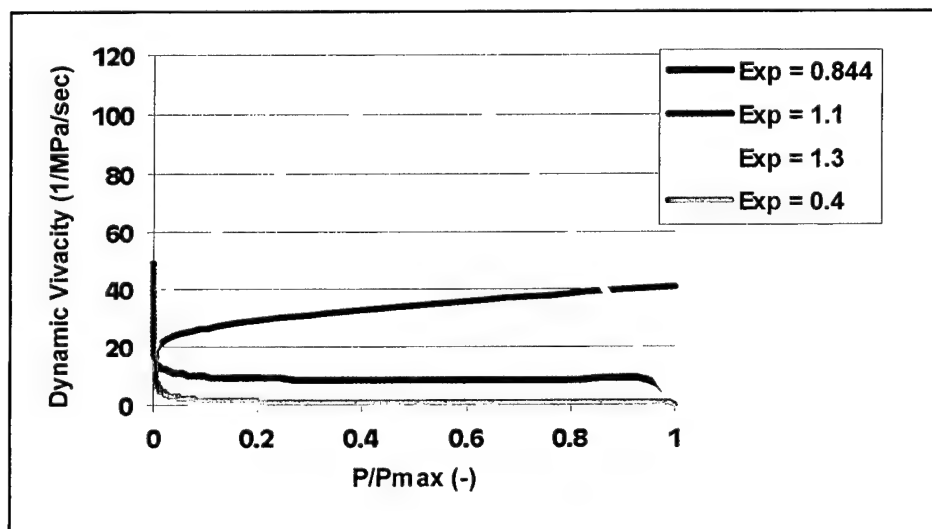
Figure 11. Dynamic Vivacity Results for Rectangular Slab Geometry for Various Burn Rate Exponents.
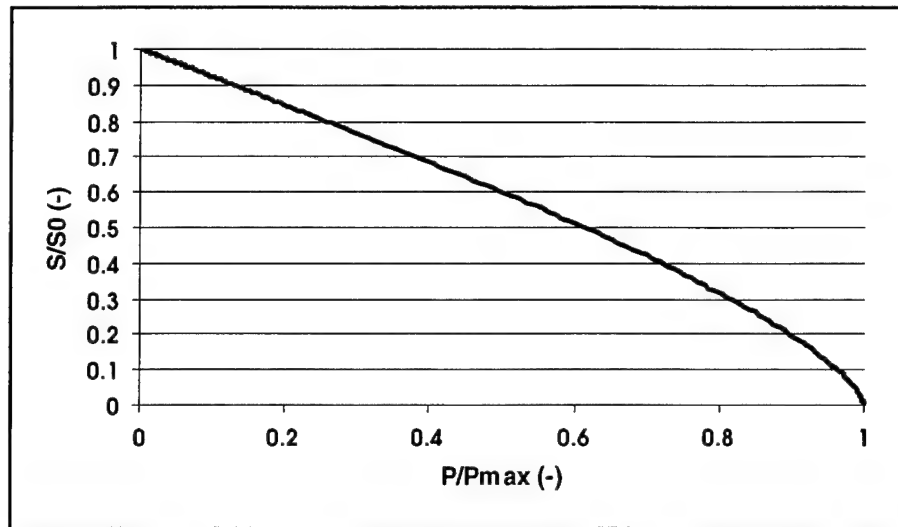
Figure 12. Surface Area Ratio for Spherical (regressive) Grain Geometry.
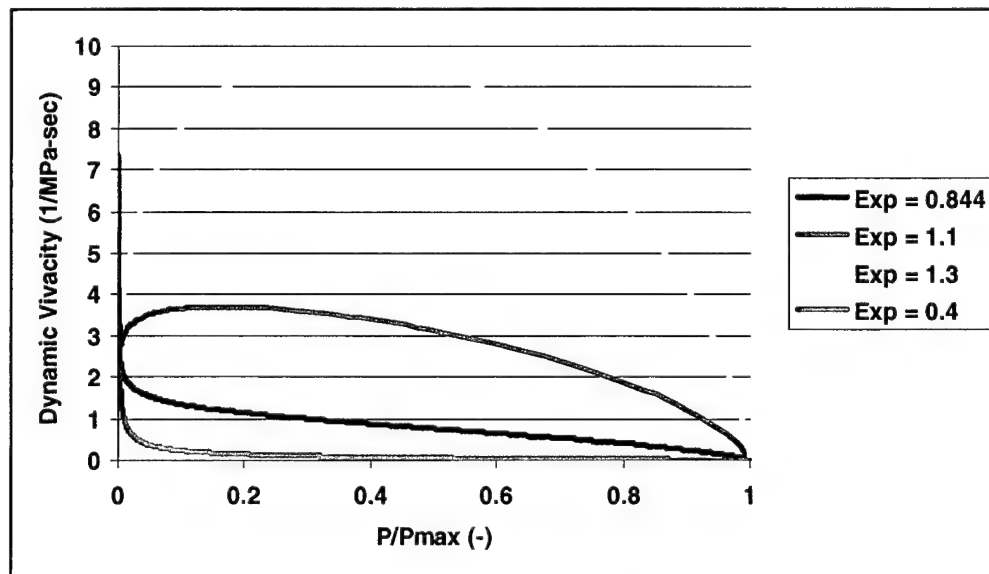
Figure 13. Dynamic Vivacity Results for Spherical Geometry for Various Burn Rate Exponents.

As indicated in Equation (19) and supported by Figures 6, 7, 8, 9, 11, and 13, the propellant burn rate exponent appears to exert a strong influence on the behavior of dynamic vivacity and the correspondence with propellant surface area. In all cases, when the propellant burn rate exponent is low (0.4), the dynamic vivacity rapidly approaches zero and no useful information concerning surface area can be determined.

Likewise, at the higher propellant burn rate exponent (1.3), the dynamic vivacity for the three cases is parabolic in structure, opening downward. Again, no meaningful information concerning propellant surface area can be deduced. Fortunately, most propellants have burn rate exponents between the other values (0.844 and 1.1) used in the simulations. Unfortunately, as indicated in the figures presented in this section and in Equation (19), once the burn rate exponent exceeds 1, the dynamic vivacity tends to result in a positive slope for the dynamic vivacity, which makes it difficult to correlate the results with the propellant surface area. If the propellant burn rate exponent is in the range of approximately 0.7 to 1, from the results shown and other calculations performed by the author given in Appendix A, the dynamic vivacity and propellant surface area appear to be in good agreement. From a practical perspective, if the burn rate of a propellant is to be determined from a closed chamber experiment and the dynamic vivacity exhibits a positive slope when the grain geometry used in the experiment is regressive and if the calculated burn rate exponent is less than 1.0, the experiment and analysis should probably be redone.

To summarize, it is not necessarily true that the slope of the dynamic vivacity will mirror the slope of the surface area curve. The propellant burn rate exponent appears to play an important role in determining the shape of the dynamic vivacity curve. However, for typical propellant burn rate exponents, the relationship between dynamic vivacity and surface area appears to track rather well. Finally, as described in [1,2,3,4] and references therein, using dynamic vivacity to determine changes in propellant composition or burning behavior by comparing the dynamic vivacity from one firing to the next of the same propellant is not impacted by the question of whether the slope of the dynamic vivacity mirrors the slope of the surface area ratio curve. This use of dynamic vivacity remains a valid and useful tool for propellant lot acceptance and determining if propellant composition has changed. The discussion addresses only the propriety of using the slope of the dynamic vivacity to determine the progressivity of the propellant geometry.

4. Sensitivity of Dynamic Vivacity to Ignition Variability

To investigate the impact of ignition variability on dynamic vivacity, closed chamber simulations will be performed with the propellant partitioned into two portions. Portion 1 will be assumed to ignite at time zero, and Portion 2 will ignite at the time that corresponds to 10% of the first portion being burned. The propellant and closed chamber parameters will be the same as used in the previous section for the burn rate exponent of 0.844. Four cases for each grain geometry are compared. The baseline case (Case 1) will have 100% of the propellant in Portion 1 (i.e., the calculation already performed in the previous section or Appendix A). Case 2 partitions the propellant with 80% in the first portion and 20% in the second portion. Case 3 will allocate 50% of the propellant to each portion. Finally, in Case 4, 20% of the propellant is placed in the first portion and 80% in the second portion. As in the previous section, three grain

geometries (progressive, neutral, and regressive) are used in the simulations. In this section, the 37-perf hexagonal geometry[4] is used for the progressive grain geometry. As in the previous section, the rectangular slab and spherical grain geometries are used for the other grain geometries.

An inspection of Figures 14 through 16 indicates that ignition delays appear to impact the dynamic vivacity during the first 0.1 of P/P_{max} and for the 37-perf hexagonal and rectangular slab grain geometry from about 0.8 of P/P_{max} forward. One can understand this behavior by examining Equation (12). Since the dynamic vivacity is graphed as a function of P/P_{max} at any given value of P/P_{max}, the burn rate, $r(t)$, in Equation (12) is the same no matter what the distribution of the propellant or the ignition delay. Thus, only the surface area term, $S(t)$, will change. Now, $S(t)$ is given by

$$S(t) = \sum_{i=1}^{N} s_i(t)\xi_i(t),\qquad(20)$$

in which $s_i(t)$ is the instantaneous surface area of an individual grain, N the total number of grains, and $\xi_i(t)$ the characteristic function for each grain.
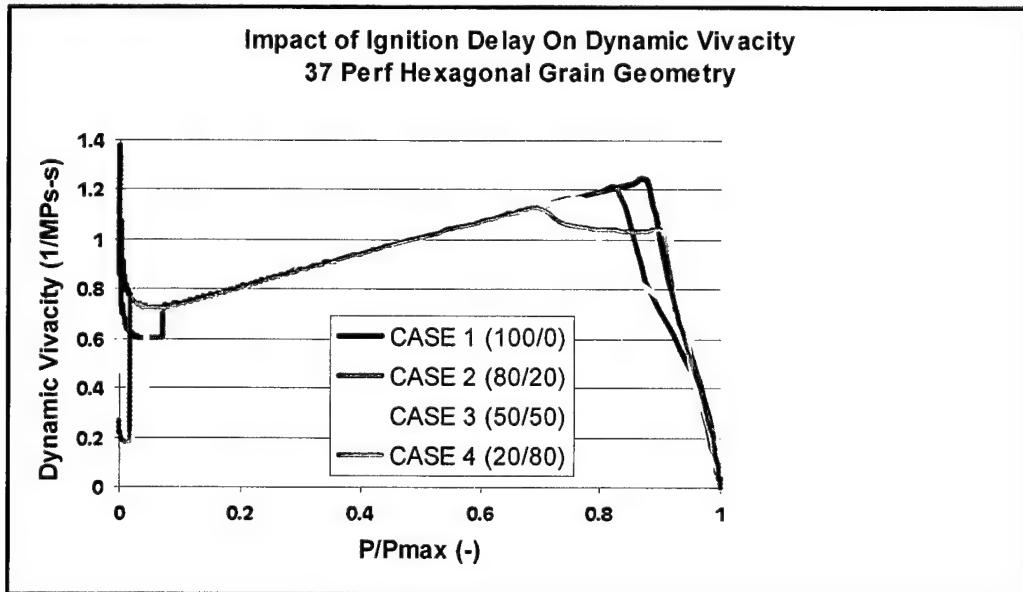

Figure 14. Dynamic Vivacity for 37-perf Hexagonal Grain Geometry With Delayed Ignition.

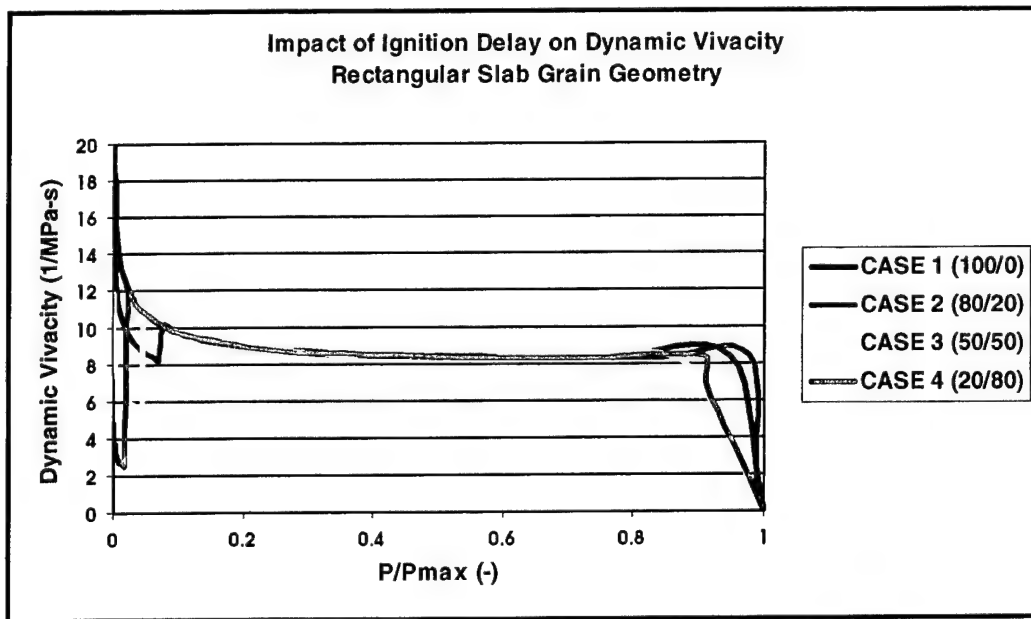[4]See Appendix A for surface area ratio and dynamic vivacity curves.

Figure 15. Dynamic Vivacity for Rectangular Slab Grain Geometry With Delayed Ignition.
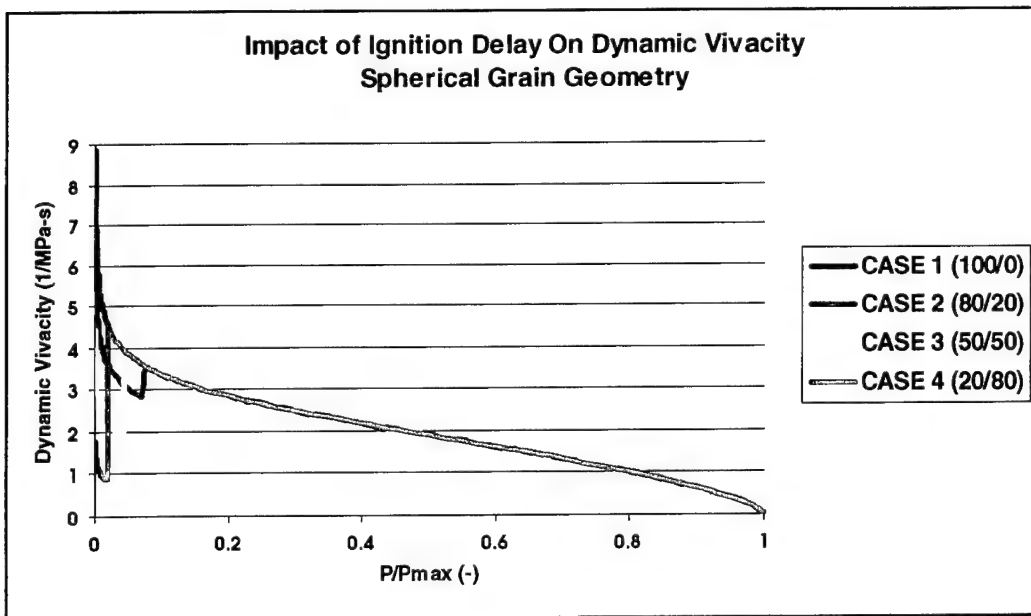

Figure 16. Dynamic Vivacity for Spherical Grain Geometry With Delayed Ignition.

16

The characteristic function is 1 if the grain is ignited and 0 otherwise. The simulation assumes that the charge was divided into two portions, $N = n_1 + n_2$, in which n_1 is the number of grains ignited at time $t = 0$ and n_2 is the number of grains in the second portion of the propellant. Thus, from Equation (12), the magnitude of the dynamic vivacity until the time/pressure when the second portion of the propellant ignites will be directly proportional to the value of n_1 since the surface area of each propellant grain in Portion 1 of the propellant charge will be the same, i.e., each grain in Portion 1 ignites at the same time and burns under the same pressure. As the percentage of the total charge in the first portion decreases, the value of n_1 decreases and the magnitude of the dynamic vivacity exhibits a corresponding larger decrease, as shown in the three figures. This explains the drop in the curves to approximately 0.1 of P/P_{max}. The fact that the curves rebound at different values of P/P_{max} is simply attributable to the conditions of the simulation. The second portion of the propellant ignites when 10% of the first portion of the propellant has burned. As the percentage of the total propellant in the first portion of the propellant decreases, the pressure generated by burning 10% of this portion will also decrease. Thus, the ignition of Portion 2 of the propellant will occur at a lower pressure, as shown in the figures. The fact that the curves coincide from approximately 0.1 to 0.8 of P/P_{max} is also a consequence of the choice of having the second portion of the propellant ignite after 10% of the first propellant portion has burned. The instantaneous surface area of two individual grains for the dimensions used in the calculations does not differ by that large of an amount if one grain starts to burn when 10% of the other grain has been consumed. This is especially true for the spherical grain geometry (see Figure 16), where the curves coincide for the entire range of P/P_{max} from approximately 0.1 to 1.

The behavior of the curves for the 37-perf hexagonal and rectangular slab grain geometries beyond about 0.8 of P/P_{max} is not as simple to explain. For the 37-perf hexagonal grain geometry, the larger the percentage of the total charge in either portion of the propellant, the closer the curve should approximate the baseline curve, i.e., the greater the percentage of propellant that ignites at the same time, the more similar the curves. For example, when 80% of the propellant is in the second portion, the curve deviates from the baseline curve at a lower value of P/P_{max}, as discussed earlier, but the total difference between the 80% curve and the baseline curve from 0.75 to 1.0 of P/P_{max} is the smallest of all the curves. Again, the larger the percentage of the total charge in either portion of the propellant, the closer the curve should approximate the baseline curve. The 50% and 20% cases are not as clear as the 80% case, but the 50% case does return to the baseline curve sooner than the 20% case. For the rectangular slab grain geometry, the behavior above approximately 0.8 of P/P_{max} is complicated by the fact that for the thickness used in the study, the grains maintain an almost constant surface area with virtually an instantaneous "burnout." Thus, the derivative for the pressure used in the calculation of the dynamic vivacity that is plotted in Figure 15 becomes sensitive to the small errors in the calculations. This can be seen by noting that in Figure 15 the curve for Case 4 at about 0.9 of P/P_{max} is not even a function. Therefore, no further analysis of the rectangular slab calculations will be given. In general, the analysis for the 37-perf hexagonal grain geometry applies to any of the grain geometries.

In the previous paragraph, the fact that the curves overlaid (coincided) from about 0.1 to 0.8 of P/P_{max} was attributed to the assumption in the simulation that the second portion of the propellant was ignited when 10% of the first portion of the propellant was consumed. To verify this claim, an additional calculation for the 37-perf hexagonal grain geometry was performed in which the propellant was divided 50-50 in each portion, but the second portion was not ignited until the first portion was 50% consumed. The results of this simulation are provided in Figure 17. The blue curve in the figure is the baseline curve from Figure 14. Note that an ignition delay such as the one used to generate Figure 17 is unrealistic for a closed chamber experiment. More realistic is the 10% delay used earlier. Based on the discussion and simulations, it appears that ignition delays will have only a marginal impact on the dynamic vivacity results, and the traditional rule of thumb of ignoring the first 10% and last 10% to 20% (depending on the degree of grain slivering) of the dynamic vivacity (and propellant burn rate) curve appears to be well justified to account for ignition variability.
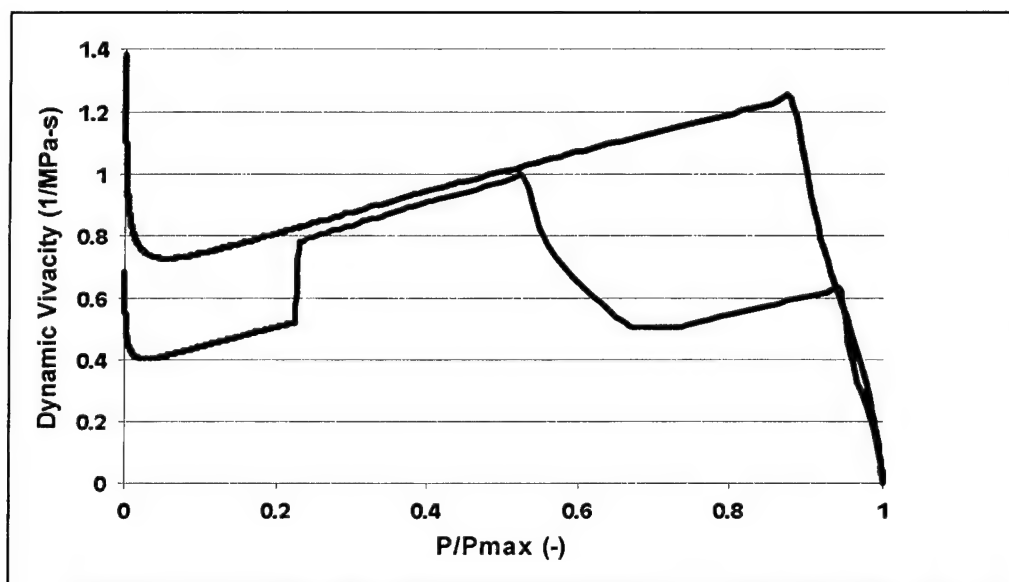
Figure 17.   Result of Delaying Ignition Until 50% of the First Propellant Portion is 50% Consumed, 37-perf Hexagonal Grain Geometry With 50-50 Distribution of Propellant.

An additional observation for the discussion concerns the sensitivity of the dynamic vivacity to the dimensions of the propellant grain geometry. If two closed chamber experiments are to be performed with the same propellant and the same propellant charge weight, then the volume of the propellant would be the same in both cases. However, if the dimensions of the propellant grains differ, even if the grain type (e.g., 7-perf cylindrical) is the same, the number of propellant grains will be different. Since volume changes as the cube of the characteristic dimension of the grain and surface area

changes as the square of the characteristic dimension, the total surface area[5], $S(t)$, will differ for the two experiments. For example, in the second experiment if the propellant is scaled by a factor of 0.5, then there will be an increase in the number of propellant grains by a factor of eight. However, the surface area of a single grain in the second case will be reduced only by a factor of 0.25. Thus, the total surface area in the second experiment will increase by a factor of 2, i.e., 8 * 0.25. From Equation (12), this would imply that the magnitude of the dynamic vivacity would also increase by a factor of 2 at every point on the dynamic vivacity curve in the second experiment, compared to the first experiment. Therefore, unlike propellant burn rate calculations that are independent of the propellant grain geometry and dimensions, the dynamic vivacity is highly dependent on both the propellant grain geometry and dimensions.

5. Sensitivity of Dynamic Vivacity to Propellant Grain Fracture

Since dynamic vivacity depends on the total surface area of the ignited propellant (see Equation [12]), grain fracture could be expected to have a significant impact on the dynamic vivacity. In general, grain fracture should result in propellant pieces that have regressive grain geometries. For example, a progressive multi-perforated grain could fracture along the perforations, creating grains with a geometry closer to that of a cord than to the multi-perforated original grain geometry. If the assumption is made that the fractured grains will result in fragments with regressive surface areas, then the graph of the dynamic vivacity for regressive grain geometries should not be dramatically affected, except possibly in terms of its magnitude. Figure 18 presents the results of dynamic vivacity simulations for a 37-perf hexagonal geometry in which 10%, 20%, 50%, and 80% of the propelling charge are assumed to disintegrate. For the calculations, the original grain dimensions are a length of 43 mm, a perforation diameter of 0.57 mm, and a web of approximately 2 mm. That portion of the charge that fractured is treated as a regressive spherical grain geometry with a diameter of 0.5 mm. It appears clear from the figure that for this choice of grain dimensions, the dynamic vivacity reflects the regressive nature of the spherical geometry to the point at which the spherical geometry is completely burned. After the consumption of the propellant spheres, the dynamic vivacity appears to parallel the curve for the baseline that assumes no grain fracture.

From Figure 18, it appears that the behavior of the dynamic vivacity was dominated by the burning of the spherical grains representing the fractured propellant. Even for substantial amounts of grain fracture (50% and 80%), the dynamic vivacity curve parallels the baseline curve, indicating that the spheres are consumed before the 37-perf hexagonal grains. Thus, the progressive nature of the non-fractured grain is still discernible. However, what would happen if the fractured propellant did not break into such small pieces as assumed in the simulations, i.e., a diameter of 0.5 mm? Results for the dynamic vivacity (assuming that the fractured propellant breaks into spherical

---

[5]Assuming uniform ignition of the propellant.

grains with larger diameters) are shown in Figure 19. In all cases, 20% of the original charge is assumed to fracture. The diameters are 0.5 mm (same as in Figure 18), 5 mm, and 10 mm. A substantial change in the dynamic vivacity can be observed for the curves with the 5-mm and 10-mm diameters. In these cases, the dynamic vivacity resembles that of a regressive or at best a neutral grain geometry. There is no indication whatsoever of the underlying progressive geometry of the 80% of the propellant that is assumed to have not suffered grain fracture.
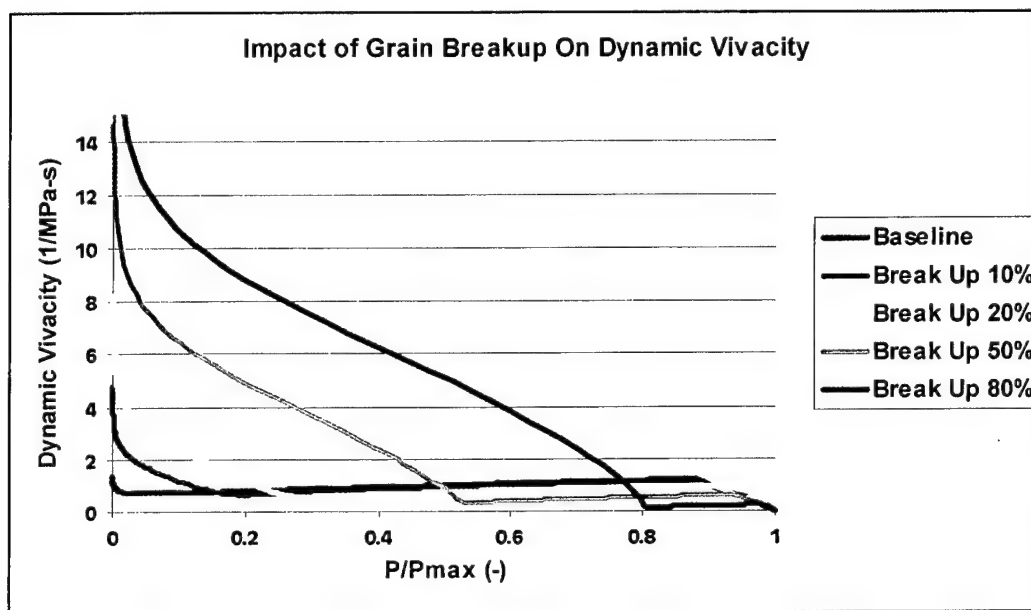

Figure 18. Dynamic Vivacity for 37-perf Hexagonal Grain Geometry, Assuming Grain Fracture for Different Percentage of Total Charge Mass.

In summary, it appears that grain fracture can significantly distort the behavior of the dynamic vivacity curve for grain geometries that are progressive. However, the distortion appears to depend on the size of the propellant pieces resulting from the fracture. Surprisingly, it is not the fracturing into small pieces that distorts the dynamic vivacity but fracturing into relatively large pieces that are present during most of the total burning time. Small fragments are consumed too fast and allow the underlying geometry of the non-fractured grains to be reflected in the dynamic vivacity curve. It is interesting to note that for reasonable propellant burn rates, the only situation that has resulted in a progressive grain geometry exhibiting a dynamic vivacity curve associated with a neutral or regressive grain geometry is when grain fracture into fairly "large" pieces occurs.
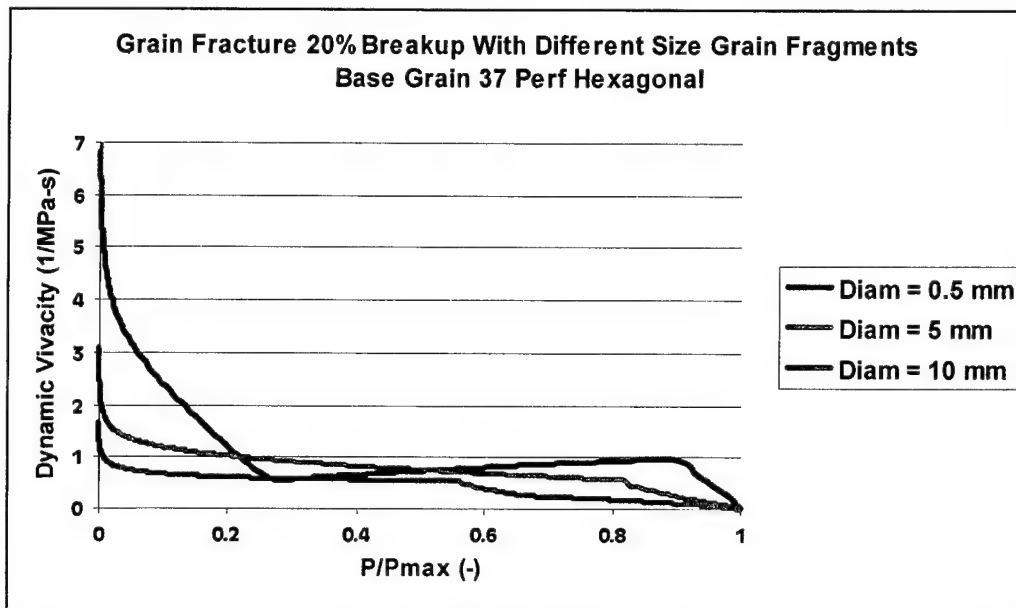
Figure 19. Dynamic Vivacity for 37-perf Hexagonal Grain Geometry, With 20% of the Propellant Assumed to Fracture Into Spheres of Different Diameters (constant diameter per simulation).

6. Dynamic Vivacity for Layered Propellant Geometries

During the past several decades, the use of a layered propellant grain geometry has been explored as a means to increase propellant gas generation progressivity. An example of a rectangular layered slab is shown in Figure 20. The basic idea is to layer a "fast" burning propellant (inner layer that generally has higher energy than the outer layer) between two slower burning propellant layers (outer layer). Once the outer layers are consumed, the inner layer ignites, producing an increased gas generation rate attributable to the higher inner layer burn rate. Essentially, for gun ballistics, the idea for this configuration is to decouple the propellant gas generation rate before and after maximum pressure. Although similar to the rectangular slab grain geometry, the surface area ratio for the layered rectangular slab exhibits a slightly different behavior as shown in Figure 21. Since the inner layer has a higher burn rate than the outer layer, the sides that have both the inner and outer layers exposed will not regress uniformly at the same rate as the top and bottom. Thus, when the outer layers are consumed, the resulting rectangular slab of inner layer material will not be a scaled version of the original as is the case for a homogeneous rectangular slab. This is reflected in the drop of the surface area ratio at about 0.3 of P/P_{max}.
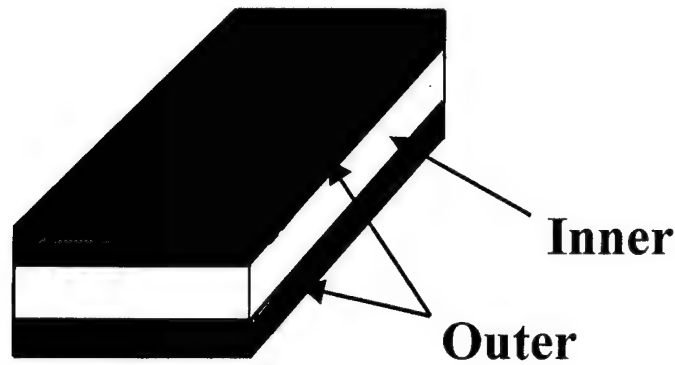
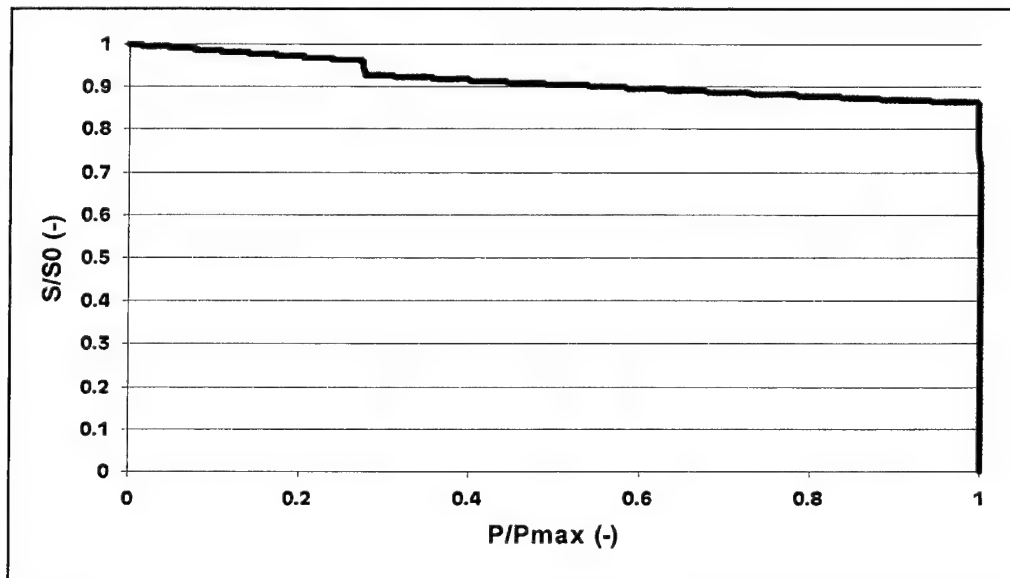Figure 20. Schematic of Layered Propellant With Slab Geometry [7].

Figure 21. Surface Area Ratio for Layered Rectangular Slab Grain Geometry.

From Equation (12), since the burn rate is a factor in the expression for the dynamic vivacity, it would appear that the dynamic vivacity for a layered geometry should increase in magnitude when the burning transitions from the outer to the inner layer. On the other hand, the surface area is reduced after the outer layer is consumed; this should have the effect of reducing the magnitude of the dynamic vivacity since surface area is also a factor in Equation (12). However, the decrease in magnitude because of the decrease in surface area should be small since the surface area for the grain geometry used in the simulation decreased by only about 10%, as indicated in Figure 21, whereas the burn rate of the inner layer is approximately 2.5 times the burn rate of the outer

layer[6]. The dynamic vivacity for this simulation is presented in Figure 22 and shows the expected increase in the magnitude of the dynamic vivacity as the burning transitions from the outer to the inner layer. However, from the figure, the increase in magnitude of the dynamic vivacity appears to exceed the increase in the burn rate between the inner and outer layer material. The least squares fit to the first portion of the data is $y(x) = 0.54095503x + 0.87923247$ and to the second portion $y(x) = 0.91854808x + 2.87199865$. To investigate the change in magnitude, the ratio of the least squares fits for the two portions of the dynamic vivacity curve is shown in Figure 23. As can be seen from the figure, the increase in magnitude of the dynamic vivacity is indeed greater than the increase in burn rate between the outer and inner layers, ranging from a factor of slightly over 3 to just below 2.7. In this example, the higher than expected value in the increase of magnitude of the dynamic vivacity is attributable to the increased specific energy or impetus of the inner layer. Often, as the specific energy of a propellant increases, the value of dP/dt also increases. To illustrate this point, the simulation for the layered propellant is performed with the specific energy and all other thermo-chemical properties of the inner layer set to the values for the outer layer. The burn rates for the outer and inner layers are the same as in the earlier simulation. Results are shown in Figures 24 and 25. The dynamic vivacity in Figure 24 is similar in structure to Figure 22, but the change in magnitude as shown in Figure 25 is within 10% (change in surface area) of the burn rate ratio between the inner and outer layers of 2.5.
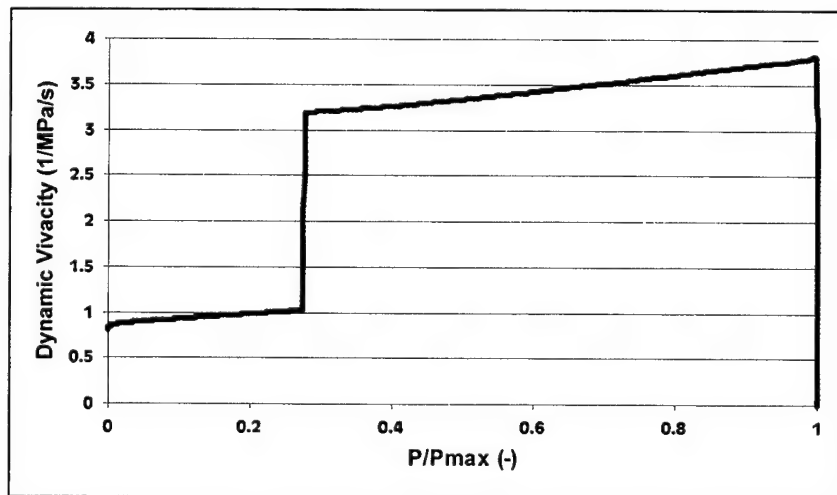

Figure 22. Dynamic Vivacity for Layered Rectangular Slab Grain Geometry.

For layered propellant geometries, it appears that the dynamic vivacity could provide relevant information concerning not only the propellant grain geometry but also the burn rate ratio between the inner and outer layers. Generally, the burn rates for the inner

---

[6]The value of 2.5 is an average over the entire pressure range and is based on an experimental propellant. The burn rates used in the simulations were $0.0407P^{1.0185}$ cm/s for the outer layer and $0.1392P^{0.9617}$ cm/s for the inner layer. The experimental propellant upon which the simulations were based had a difference in impetus of 26% (1075 J/g versus 1356 J/g) between the outer and inner layers.

and outer layer propellants are determined in a non-layered configuration, i.e., homogenous grains of inner and outer layer material. If the magnitude of the dynamic vivacity when evaluated in the layered configuration does not have approximately[7] the same ratio (outer to inner layer burning) as the computed burn rate ratio for the individual layers, then the layered propellant should be examined to determine if the burn rate ratio between the layers is being maintained. For example, migration of material between the outer and inner layers could affect the burn rates of the individual layers.
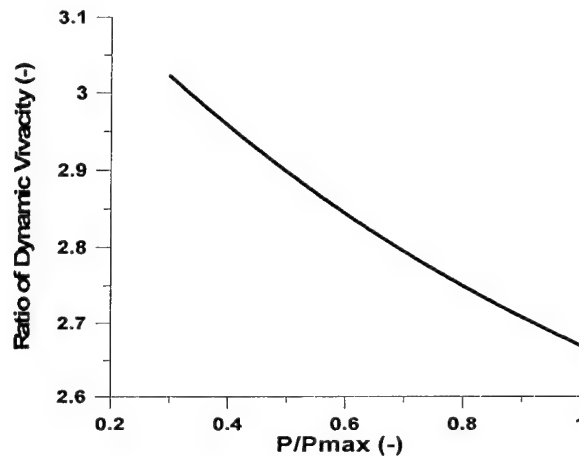

Figure 23. Ratio of Dynamic Vivacity for High and Low Portions of the Dynamic Vivacity Curve After the Consumption of the Outer Layers.
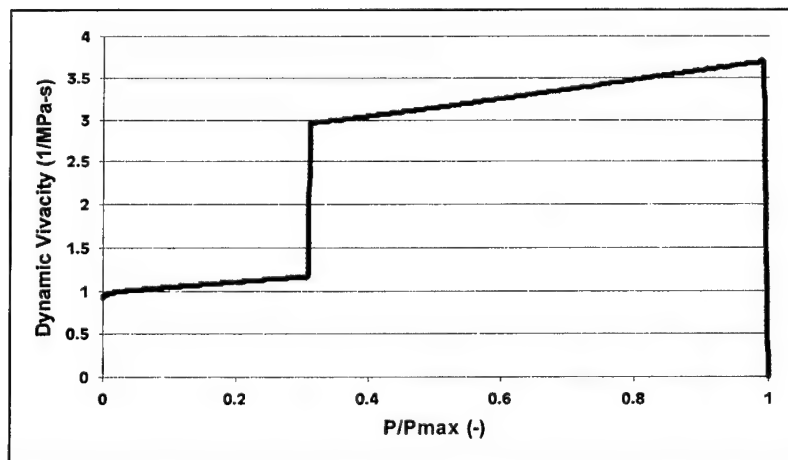

Figure 24. Dynamic Vivacity for Layered Rectangular Slab Geometry With the Specific Energy of the Inner and Outer Layers the Same.

---

[7]This statement must be used as a guideline since the ratio is impacted by the thermochemical properties of the inner and outer layers as illustrated.
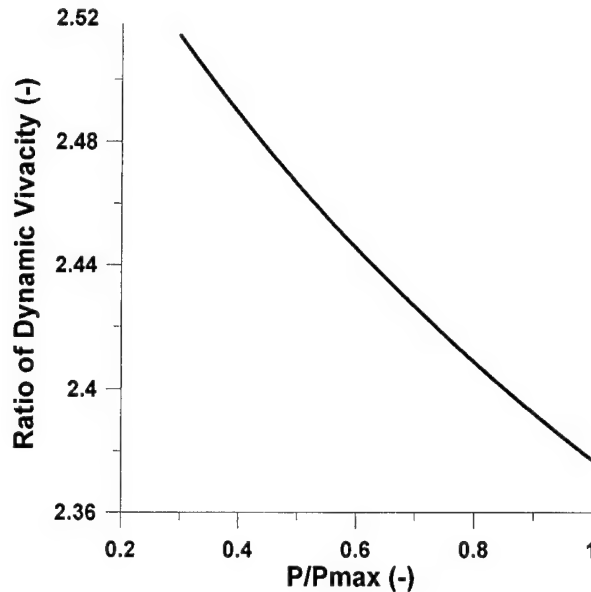
24

Figure 25. Ratio of Dynamic Vivacity for High and Low Portions of the Dynamic
Vivacity Curve After the Consumption of the Outer Layers. (Specific energy
of the inner and outer layers is the same.)

7. Dynamic Vivacity in ETC Closed Chamber Experiments

In an ETC closed chamber experiment, thermal energy is added to the chamber in the form of a plasma. The thermal energy is obtained from electrical energy through ohmic heating of the plasma. However, for the simulations performed in this study, the input electrical energy is not added as thermal energy in the form of a plasma but simply as thermal energy as represented by an increase in the mean gas temperature. Thus, the calculations do not account for any possible changes in the gas kinetics and the associated impact on propellant burn rate and pressurization rates. Nevertheless, the simulations should provide insight into the interpretation of dynamic vivacity for ETC closed chamber data. For all the simulations, a square electrical power (electrical energy/time) pulse (i.e., constant electrical power) is used.

The baseline calculation is for the 37-perf hexagonal grain geometry without the addition of any electrical energy, which was presented earlier. Three ETC simulations are presented. For each of the ETC simulations, the propellant information and mass are the same as for the baseline case; the difference is in the amount and duration of the electrical (thermal) energy added to the simulation. The first simulation adds 30 kJ of electrical energy in 1 ms, the second case adds 60 kJ in 1 ms, and the third simulation adds 30 kJ in 0.5 ms. In the simulation, the propellant mass is 60 grams. Thus, the electrical energy density is 1 kJ/g or 2 kJ/g, which are typical electrical energy densities for ETC closed chamber experiments. In addition, the total chemical energy in the propellant is ~330 kJ.

Pressure histories for the four simulations are shown in Figure 26. As one might expect, the greater the electrical power, the shorter the pressure rise time. Also, the maximum pressure increases as the total amount of added electrical energy is increased. The maximum pressure for the baseline case is 497 MPa; for the addition of 30 kJ of electrical energy, the maximum pressure is 543 MPa; and finally, when 60 kJ of electrical energy are added, the maximum pressure is 589 MPa. Since the simulations are performed with the assumption of no losses, the delta in pressure for the case of no electrical energy added to 30 kJ should be the same as for the case from 30 kJ to 60 kJ of added electrical energy. In both cases, the pressure difference is 46 MPa. Based on the pressure histories, it would be natural to assume that dP/dt would increase as the power increases. However, this relationship does not hold, as shown in Figure 27. The results of Figure 27 might be explained as a combination of several effects. The first is a consequence of treating the electrical energy as a mass less thermal energy source. From the Nobel-Abel equation of state, the pressure is a function of the product of the number of moles of gas and the mean gas temperature. Thus, energy added by burning propellant is more efficient in producing pressure since it produces moles of gas as well as temperature. Added electrical energy only increases the mean gas temperature. Therefore, at a given pressure, the most efficient use of the energy (as measured by dP/dt) will be for the case in which the added electrical energy is the least. This is illustrated in Figure 27. The second effect is suggested by Homan (private communication, Aberdeen Proving Ground, Maryland, September 2001). Referring to Figure A-11 of Appendix A, the surface area for a 37-perforation hexagonal grain geometry is strictly increasing until the point of grain slivering. Now referring to Figure 27, at any given pressure, the depth of the burned grain will increase as the electrical energy input decreases since the total required energy for a given pressure is approximately the same for all four cases. The greater the surface area, the larger the value of dP/dt since more moles of gas will be generated during the time step. This explanation is supported by the results shown in Figure 27.
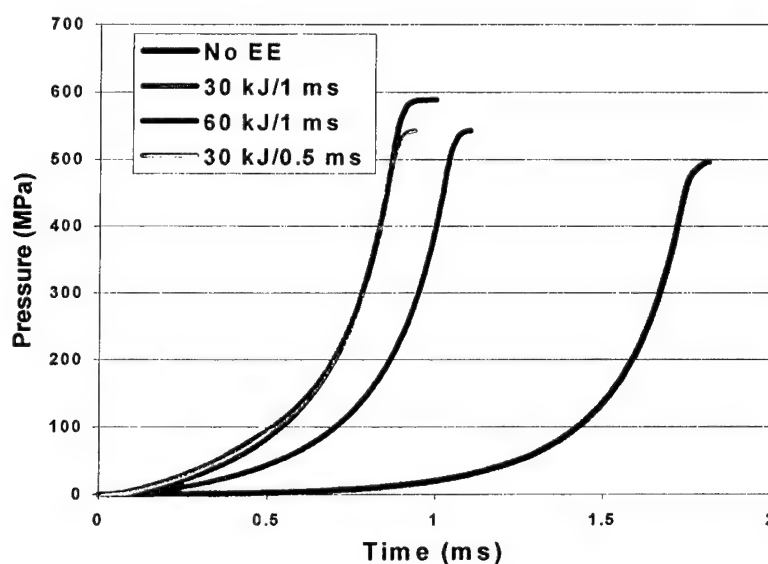

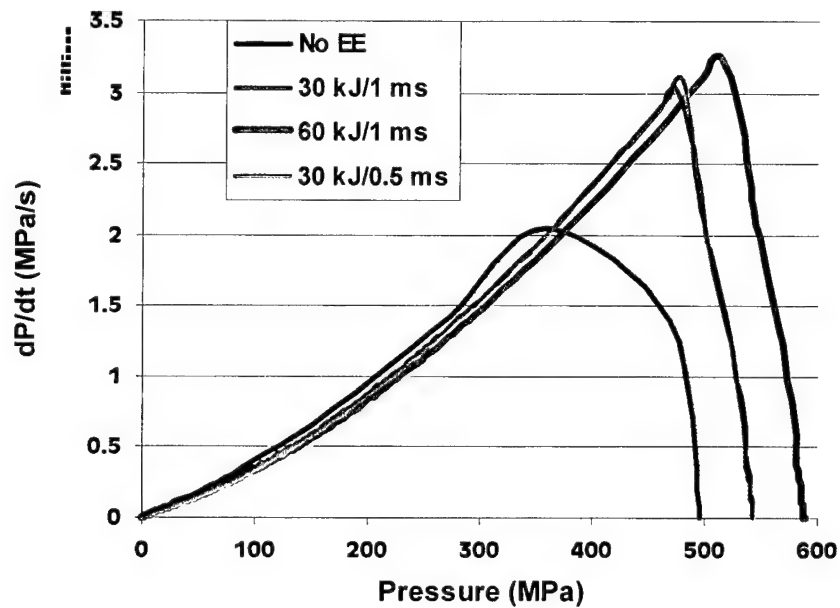Figure 26. Pressure Histories for ETC Closed Chamber Simulations.

Figure 27. Pressure Derivatives for the Four Cases Investigated in the ETC Simulations.

Given that dP/dt decreases and the maximum pressure increases as the amount of added electrical energy increases, the dynamic vivacity should be expected to decrease in magnitude as the amount of electrical energy increases. The dynamic vivacity results are shown in Figure 28.
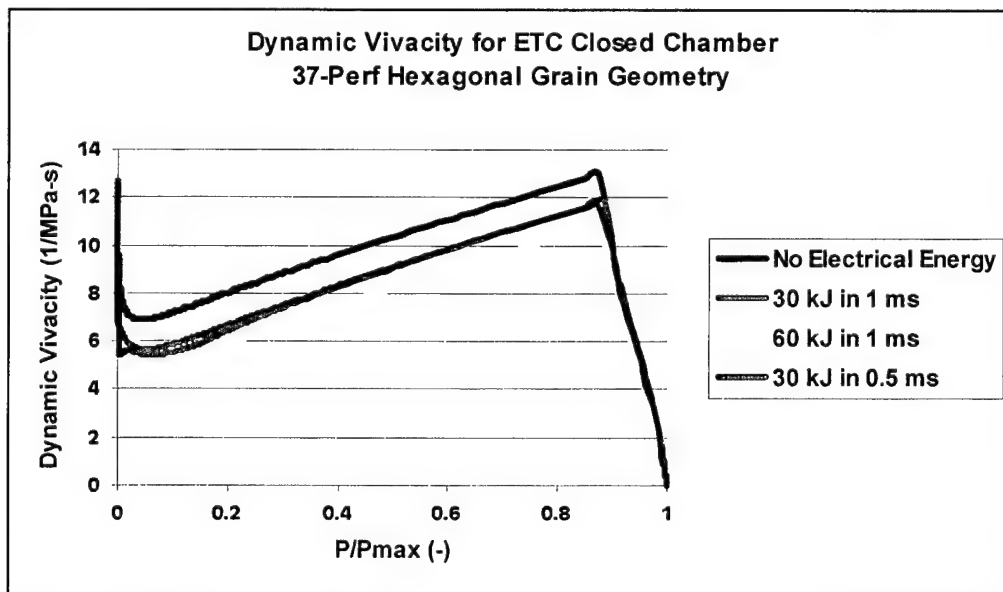

Figure 28. Dynamic Vivacity for ETC Closed Chamber Simulations.

Although the magnitude of the dynamic vivacity decreased as expected with the increased electrical energy, the basic shape of the dynamic vivacity curve remains unchanged for the different cases. Thus, it appears that for ETC closed chamber experiments, the addition of electrical energy does not impact the propriety of using dynamic vivacity to explore the surface area behavior of the propellant, at least for the assumptions made in the simulations. Therefore, no special manipulation of the data (e.g., correcting pressure to eliminate the effect attributable to the electrical energy) appears to be necessary for ETC closed chamber data in order to obtain meaningful information concerning grain geometry.

8. Summary

As stated in the introduction, the objective of this work was to (a) examine the physical meaning of the dynamic vivacity as defined in Equation (1); (b) theoretically explore the behavior of the dynamic vivacity for conventionally ignited charges of various geometries, including layered propellant charges; and (c) determine the appropriate method for applying dynamic vivacity to ETC closed vessel data. Physically, the dynamic vivacity has no simple interpretation, depending on the physical properties of the propellant including its thermo-chemical properties, density, burn rate, instantaneous surface area, and closed chamber pressure, as given in Equation (12). From the analysis, the dynamic vivacity is sensitive to the burn rate exponent appearing in Vielle's Law. Other conclusions from this study follow.

If the dynamic vivacity is to be used as an indication of propellant grain surface area behavior, then it appears to be a robust statistic to use as long as the burn rate exponent of the propellant is in the range of approximately 0.7 to 1. For exponents in this range, the dynamic vivacity appears to mirror the propellant grain geometry, even for realistic propellant ignition delays and modest grain fracture. If the exponent drops below ~0.7, the dynamic vivacity will approach zero no matter what the nature of the grain geometry. Once the burn rate exponent exceeds 1.0, the dynamic vivacity tends to exhibit the behavior of a progressive grain geometry. From a practical perspective of interpreting closed chamber data, if the burn rate of a propellant is to be determined, if the dynamic vivacity exhibits a positive slope when the grain geometry used in the experiment is regressive or neutral, and if the calculated burn rate exponent is <1.0, the experiment and analysis should be redone.

As mentioned in the previous paragraph, ignition delays appear to have only a marginal impact on the dynamic vivacity results. The traditional rule of thumb of ignoring the first 10% and last 10% to 20% (depending on the degree of grain slivering) of the dynamic vivacity (and propellant burn rate) curve appears to be well justified and adequate to account for ignition variability.

Grain fracture appears to significantly distort the behavior of the dynamic vivacity curve for progressive grain geometries. However, the distortion appears to depend on the size of the propellant pieces resulting from the fracture. Surprisingly, it is not the fracturing into small pieces that distorts the dynamic vivacity but the fracturing into relatively large pieces that are present during most of the total burning time. Small fragments burn too fast and allow the underlying geometry of the non-fractured grains to be reflected in the dynamic vivacity curve. It is interesting to note that the only situation encountered in this study that resulted in a progressive grain geometry exhibiting a dynamic vivacity curve associated with a neutral or regressive grain geometry was when the grain fractured into fairly "large" pieces.

The dynamic vivacity is highly dependent on both the propellant grain geometry and dimensions. This is unlike propellant burn rate calculations that are essentially independent of the propellant grain geometry and dimensions. For layered propellant geometries, the dynamic vivacity appears to provide relevant information about the propellant grain geometry as well as the burn rate ratio between the inner and outer layers. The dynamic vivacity for ETC closed chamber experiments appears to accurately reflect the propellant grain geometry independently of the amount or timing of the added electrical energy. No modifications of the dynamic vivacity calculation to account for the electrical energy are required.

In summary, based on the results of this study, the dynamic vivacity provides a very stable indicator of propellant geometry in the closed chamber experiment. A discussion of other important uses of the dynamic vivacity in propellant lot acceptance and quality testing is presented in the references. Ignoring propellants with unrealistic burn rate exponents (i.e., < 0.7), only two cases were encountered in this study in which the dynamic vivacity did not reflect the propellant grain geometry. The first case occurs when the burn rate exponent of the propellant exceeds 1.0. In this case, neutral and regressive grain geometries could produce dynamic vivacity curves indicating a progressive grain geometry. Given the new class of experimental propellants with burn rate exponents exceeding 1.0, it is recommended that burn rate and dynamic vivacity calculations be examined closely for consistency. The second case involves dynamic vivacity curves for progressive grain geometries that indicate neutral or regressive grain geometries. In this case, grain fracture into relatively "large" pieces may have occurred. Not addressed in this report is the impact on the dynamic vivacity that would occur if in-depth burning occurs or if the propellant is "poorly" manufactured. Specifically, what will be the result if the propellant density is significantly below its theoretical mean density? Finally, because of the robust nature of the dynamic vivacity exhibited during this study, it is recommended that any data analysis or the quality of the propellant manufacturing associated with a closed chamber experiment for which the dynamic vivacity curve appears in any way unusual should be questioned and re-examined.

INTENTIONALLY LEFT BLANK

References

1. Bannatyne, J.C., *The Closed Vessel and Its Use in Acceptance Testing of Gun Propellants*, Proof and Experimental Services Technical Memorandum Quality Assurance Branch, Materiel Command, Department of National Defense, Hull, Quebec, September 1968.

2. Grivell, M.R., *The Closed Vessel Test and Determination of Ballistic Properties of Gun Propellants* Manual WSRL-0291-MA, Defence Science and Technology Organisation, Weapons Systems Research Laboratory, Defence Research Centre Salisbury, South Australia, November 1982.

3. Klingaman, K.W., and J.K. Doman, "The Role of Vivacity in Closed Vessel Analysis," *Proceedings of the 1994 JANNAF Propellant Development and Characterization Subcommittee Meeting*, AD-B187 111 (95-0170) pp. 149–159, NASA Kennedy Space Center, FL, April 1994.

4. Machalka, E., "Programmes for the Determination of Propellant Characteristics in Conjunction with Closed Vessels," special edition of *Proceedings of the 3rd International AVL Symposium on Ballistics*, Graz, Austria, 30 August to 3 September 1982.

5. Nobel, A., and F.A. Abel, "Researches on Explosives-Fired Gun-powder," *Philosophical Transactions of the Royal Society, Vol. 165*, London, 1875.

6. Anderson, R.D., and K.D. Fickie, *IBHVG2 – A User's Guide*, BRL-TR-2829, U.S. Army Ballistic Research Laboratory, Aberdeen Proving Ground, MD, July 1987.

7. Oberle, W.F., *Methodology for Determining Propellant Charge Dimensions for Layered Propellant Charges*, ARL-TN-178, U.S. Army Research Laboratory, Aberdeen Proving Ground, MD, May 2001.

INTENTIONALLY LEFT BLANK

Symbols		Units
A	dynamic vivacity	1/(Pa-sec)
b	propellant covolume	m^3/kg
$dP(t)/dt$	time derivative of pressure	Pa/sec
d	propellant loading density	kg/m^3
M	gas molecular weight	
m_0	initial propellant mass	kg
N	total number of propellant grains	
n_1	number of grains in Portion 1	
n_2	number of grains in Portion 2	
$n(t)$	moles of gas	(-)
$P(t)$	pressure	Pa
P_{max}	maximum pressure	Pa
R	universal gas constant	J/kg-K
$r(t)$	propellant burn rate	m/s
$S(t)$	propellant surface area	m^2
$s_i(t)$	surface area of a single grain m^2	
T	gas temperature	K
V_0	initial chamber volume	m^3
V_p	initial propellant volume	m^3
$z(t)$	mass fraction burned	(-)
α	burn rate exponent	(-)
β	burn rate coefficient	m/sec-Pa$^\alpha$
ρ	propellant density	kg/m^3
$\xi_i(t)$	grain characteristic function	

INTENTIONALLY LEFT BLANK

APPENDIX A

SURFACE AREA AND DYNAMIC VIVACITY FOR
VARIOUS PROPELLANT GEOMETRIES

INTENTIONALLY LEFT BLANK

SURFACE AREA AND DYNAMIC VIVACITY FOR VARIOUS PROPELLANT GEOMETRIES

The IBHVG2 interior ballistic code [6] used to perform the simulations in this report supports 14 different grain geometries: cord, rectangular slab, sphere, slotted stick, single perforation, 7-perf, 19-perf, 19-perf hexagonal, 37-perf hexagonal, rosette grain, rolled ball grain, star grain, monolithic multiple perf grain, and a general grain. The surface area ratio and dynamic vivacity for the rectangular slab, sphere, and 19-perf grain were presented in Section 2. Similar calculations for all but the last two grain geometries are provided in this appendix.
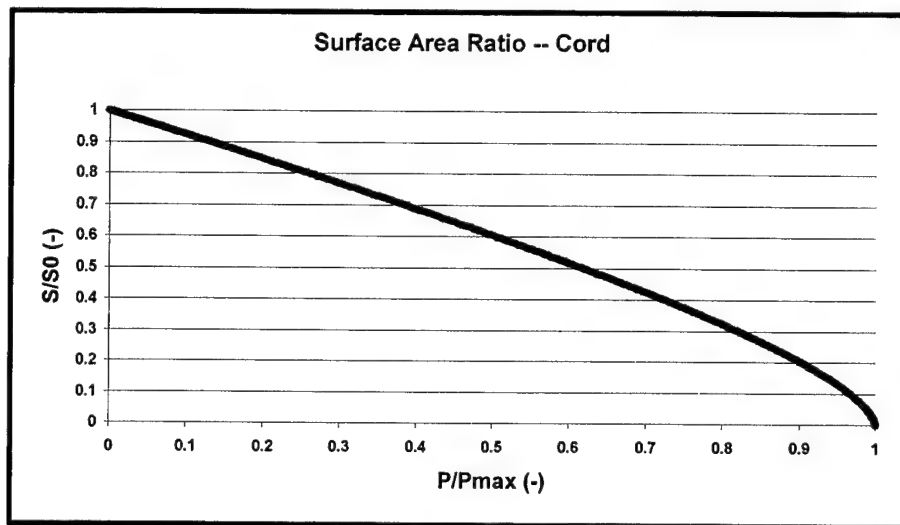
Figure A-1. Surface Area Ratio for Cord Geometry.
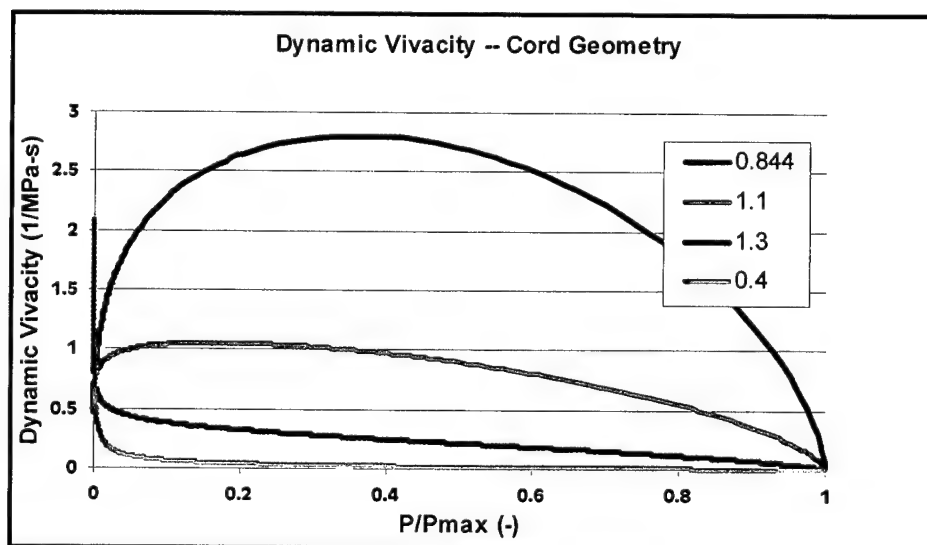
Figure A-2. Dynamic Vivacity for Cord Geometry.
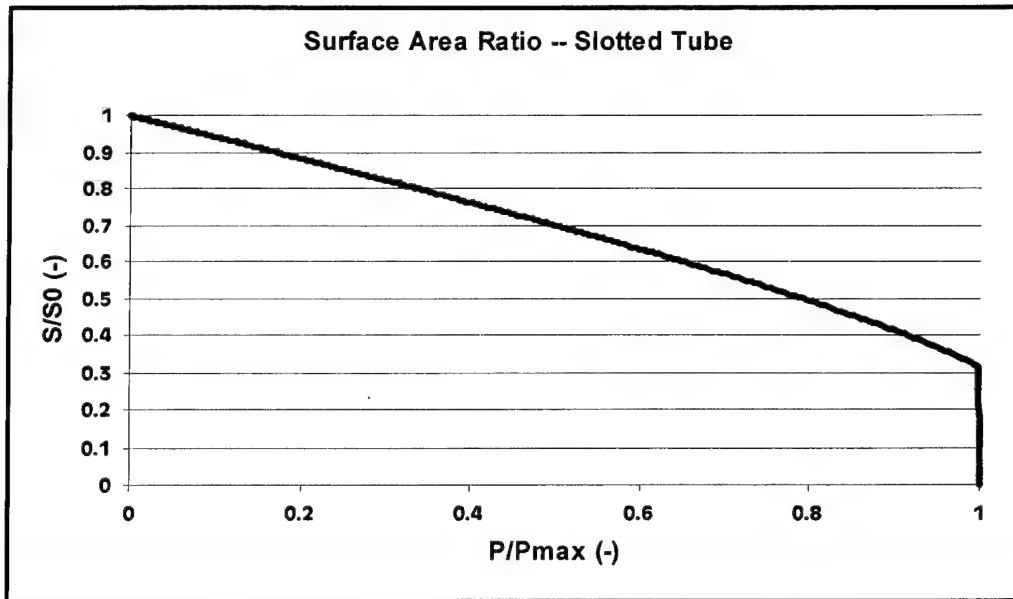
Figure A-3. Surface Area Ratio for Slotted Stick.
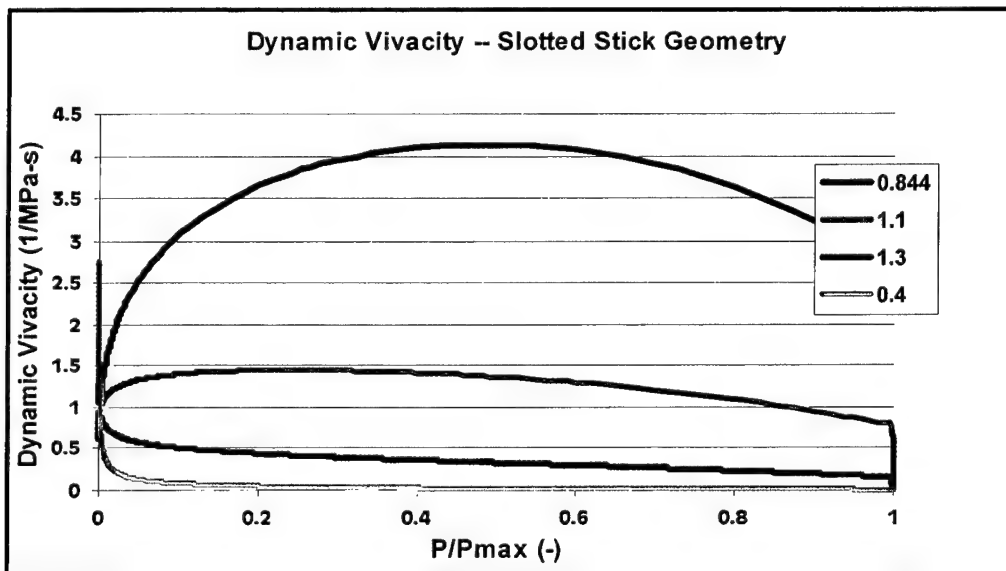
Figure A-4. Dynamic Vivacity for Slotted Stick.
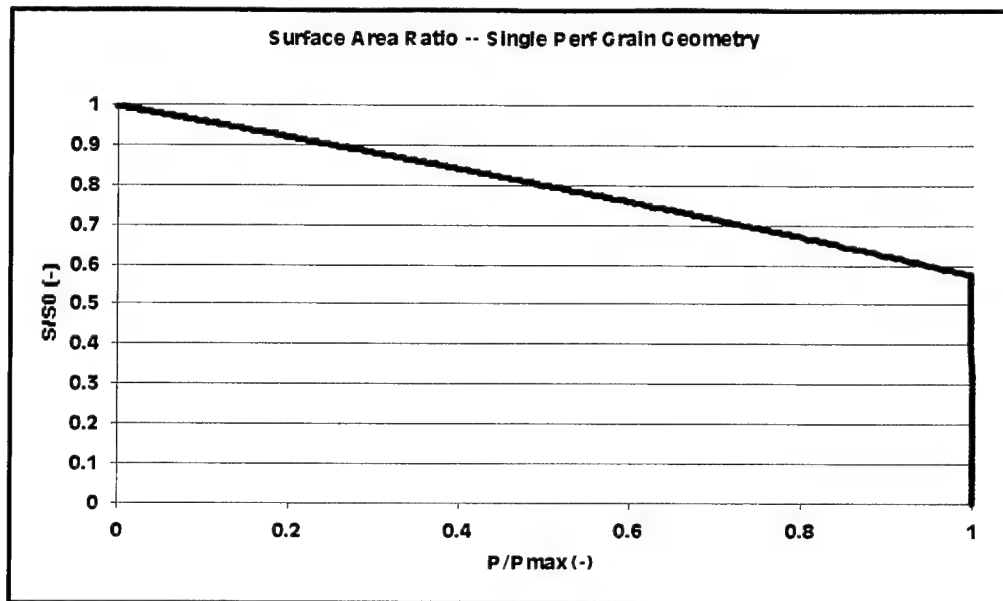
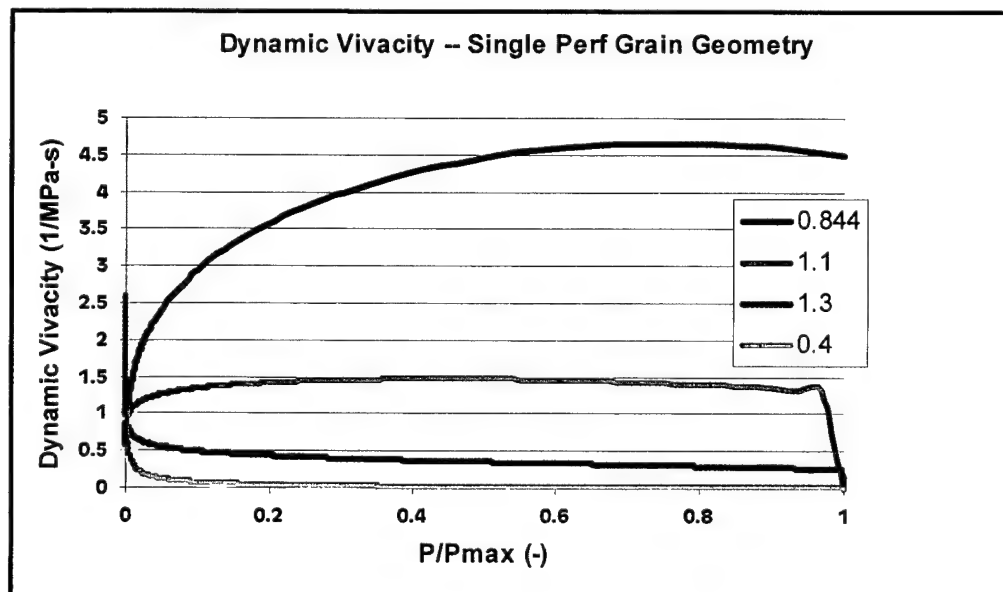Figure A-5. Surface Area Ratio for Single Perforated Grain.

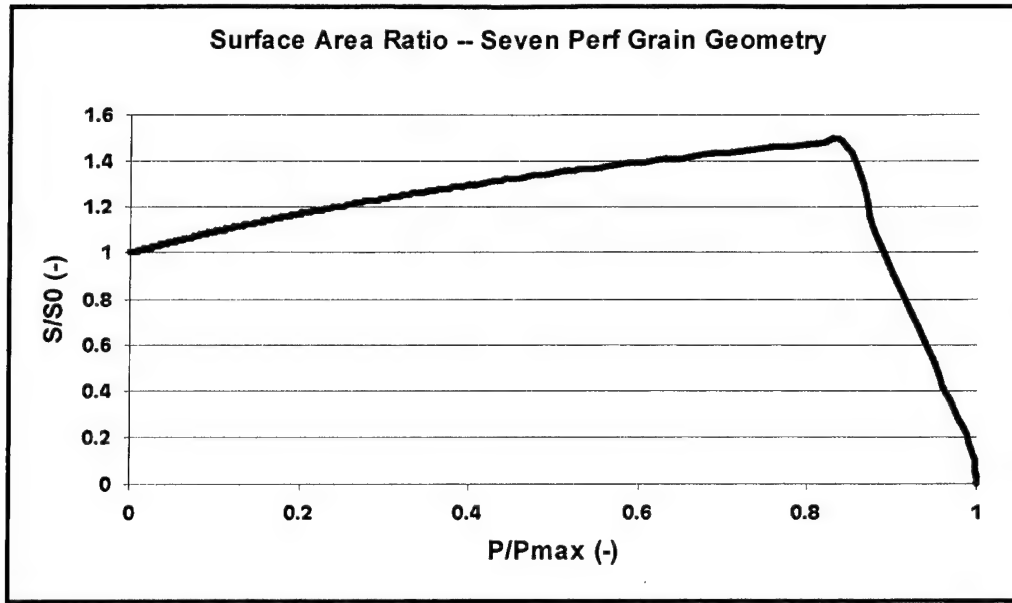Figure A-6. Dynamic Vivacity for Single Perforated Grain Geometry.

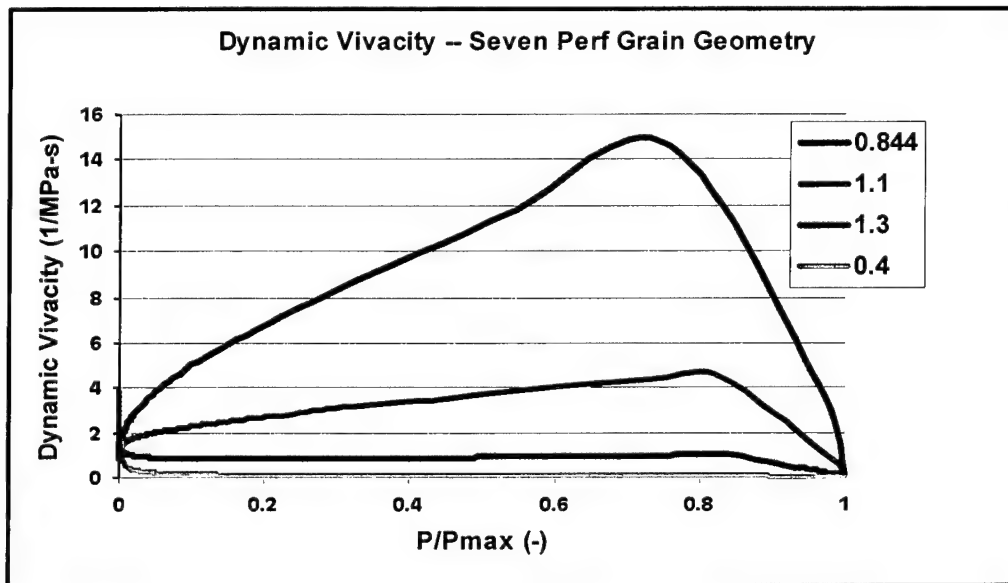Figure A-7. Surface Area Ratio for 7-perf Grain Geometry.

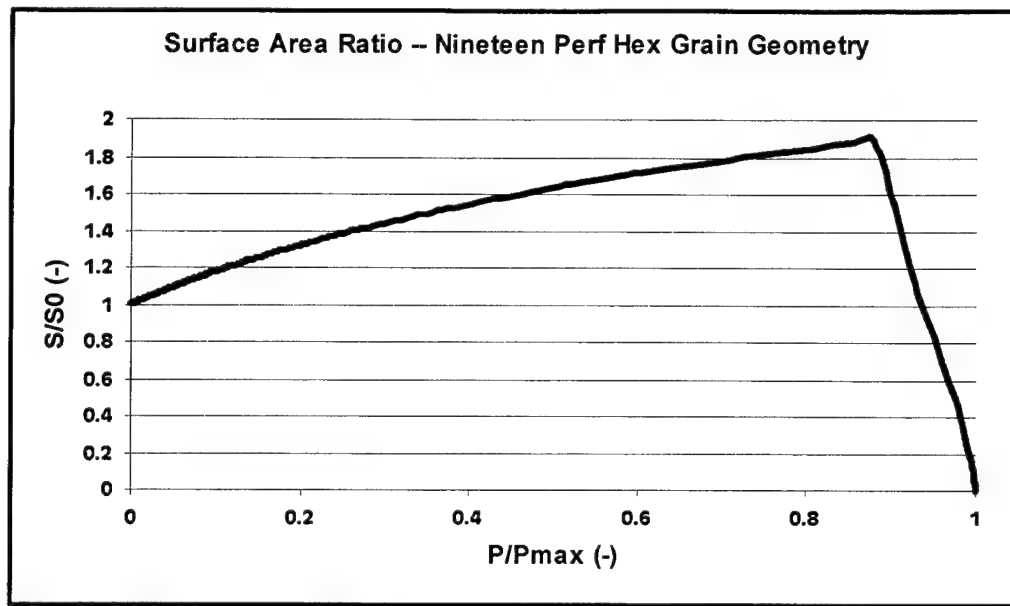Figure A-8. Dynamic Vivacity for 7-perf Grain Geometry.

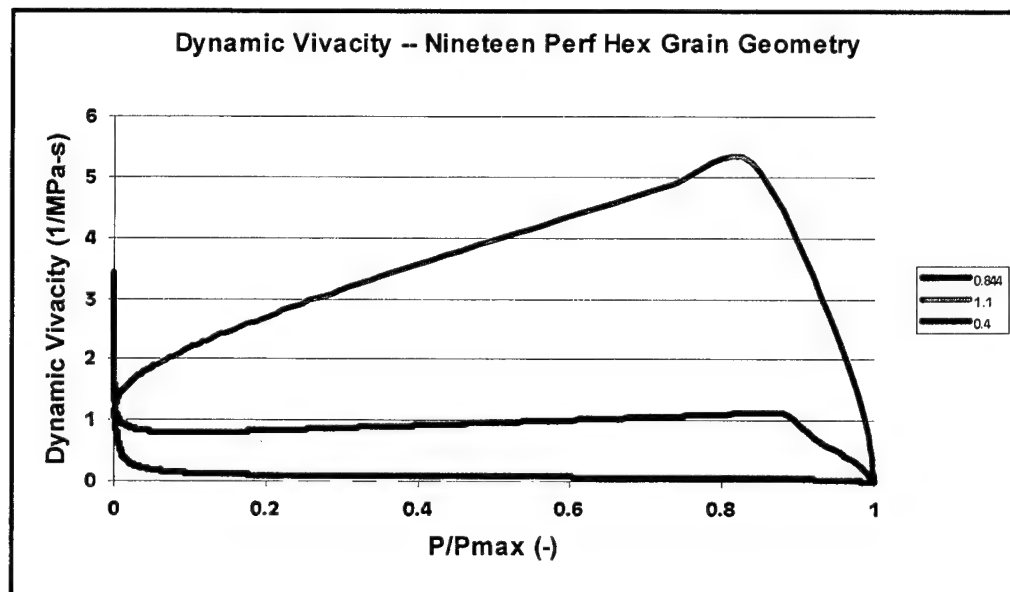Figure A-9. Surface Area Ratio for 19-perf Grain Geometry.

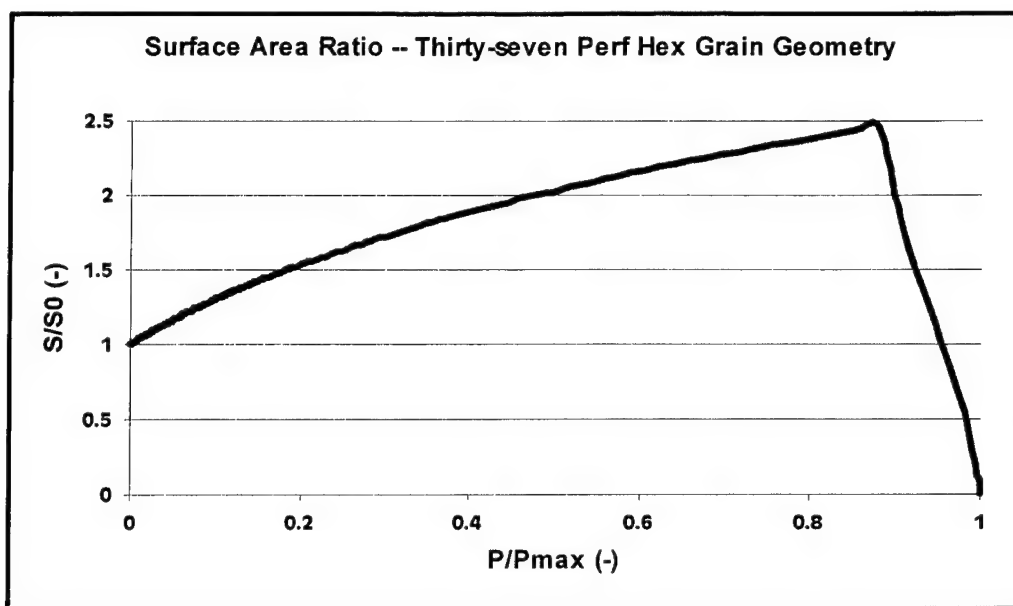Figure A-10. Dynamic Vivacity for 19-perf Hexagonal Grain.

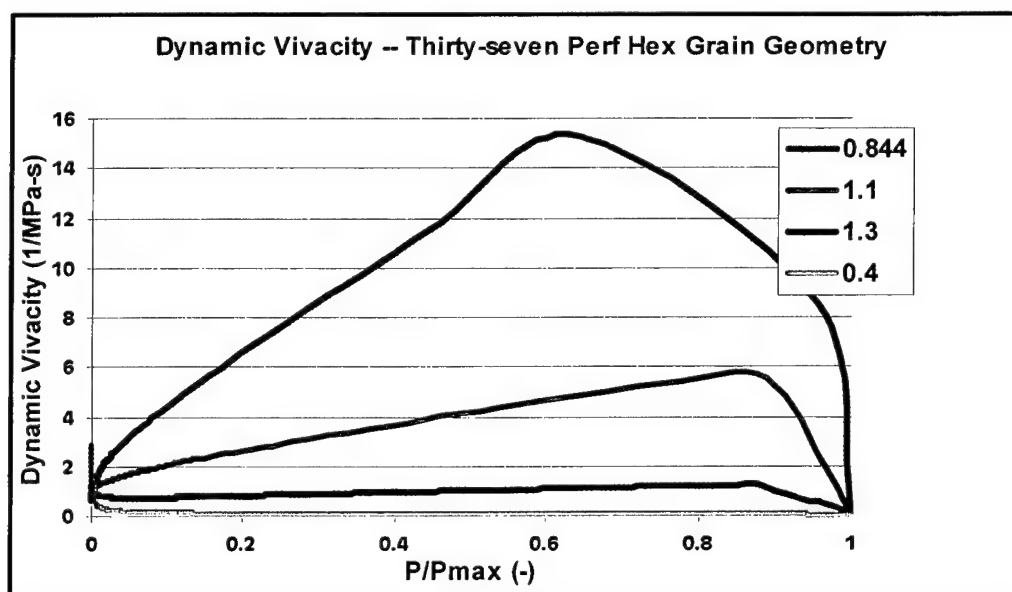Figure A-11. Surface Area Ratio for 37-perf Hexagonal Grain.

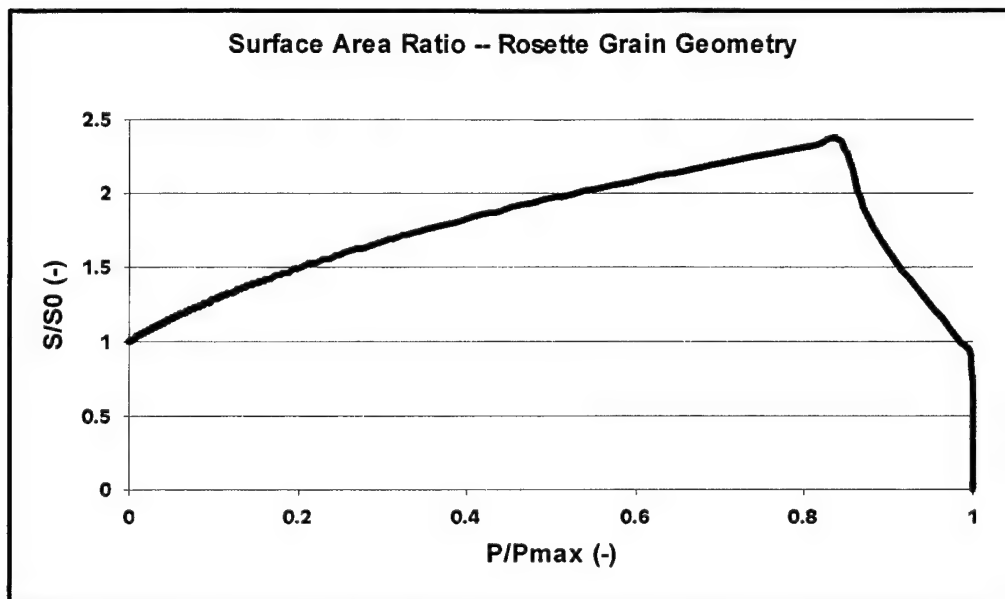Figure A-12. Dynamic Vivacity for 37-perf Hexagonal Grain.

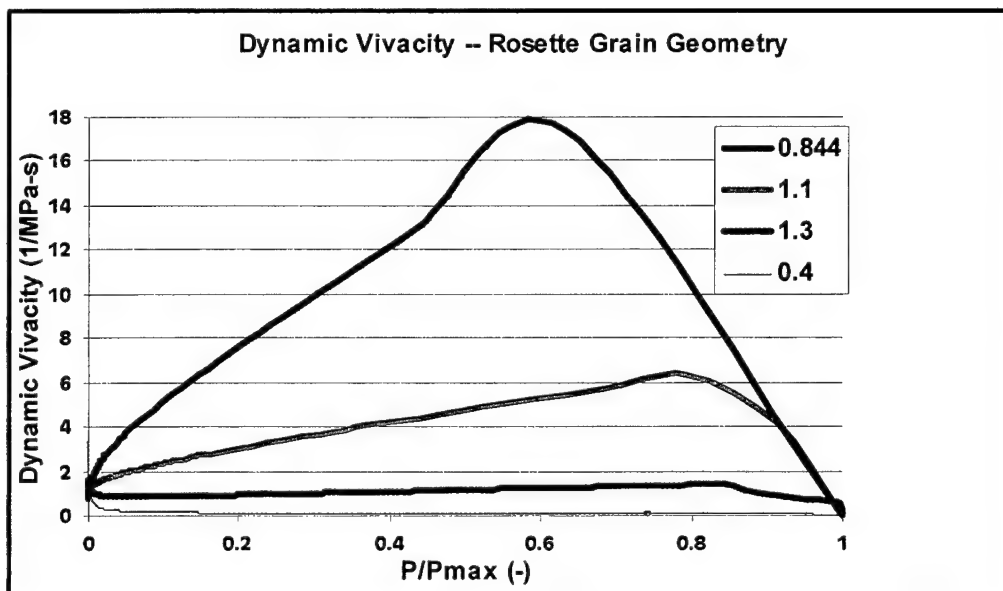Figure A-13. Surface Area Ratio for Rosette Grain.

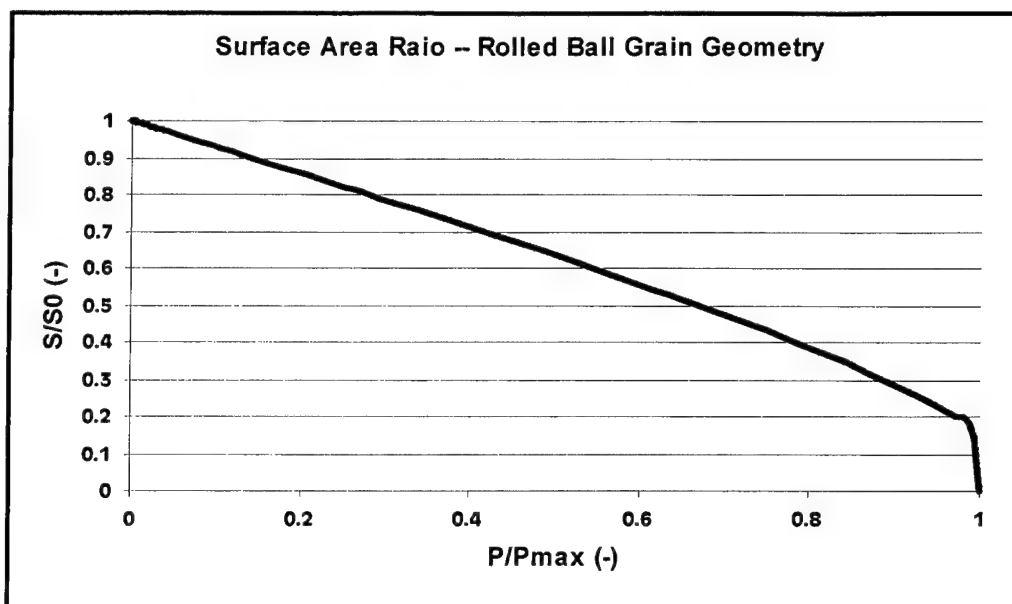Figure A-14. Dynamic Vivacity for Rosette Grain Geometry.

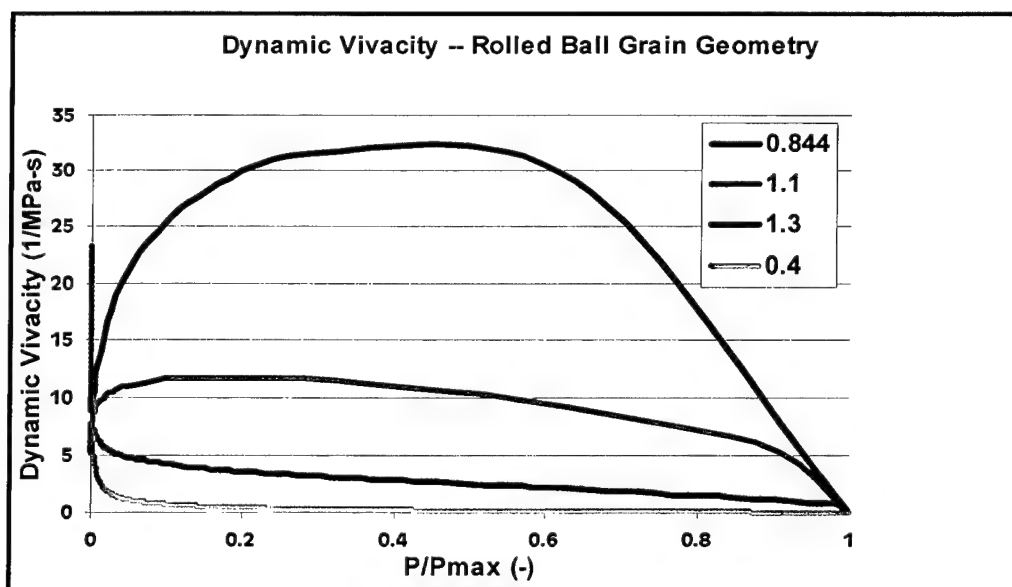Figure A-15. Surface Area Ratio for Rolled Ball Grain.

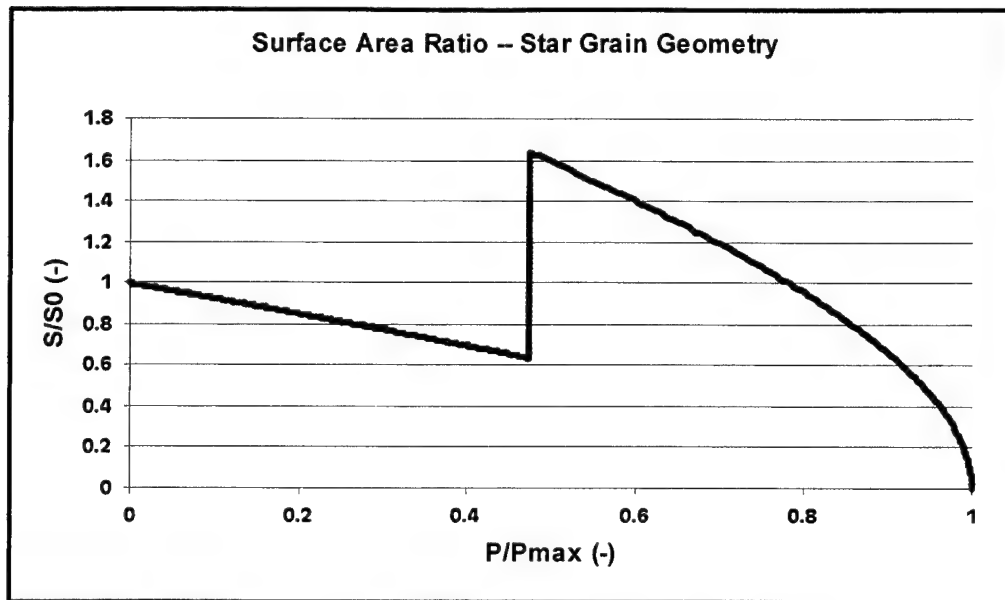Figure A-16. Dynamic Vivacity for Rolled Ball Grain Geometry.

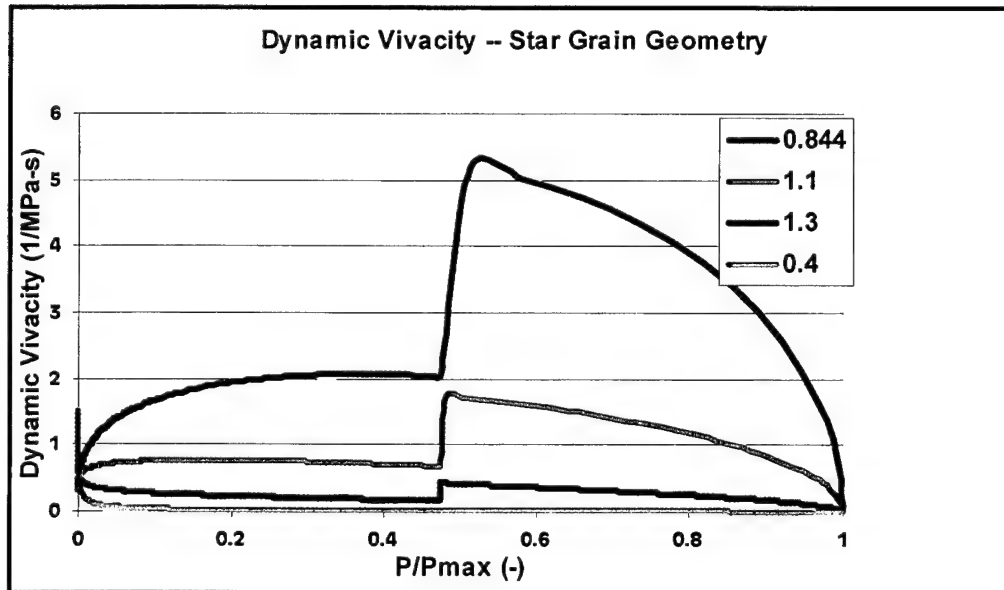Figure A-17. Surface Area Ratio for Star Grain Geometry.

Figure A-18. Dynamic Vivacity for Star Grain Geometry.

INTENTIONALLY LEFT BLANK

NO. OF
COPIES   ORGANIZATION

1   ADMINISTRATOR
    DEFENSE TECHNICAL INFO CTR
    ATTN DTIC OCA
    8725 JOHN J KINGMAN RD STE 0944
    FT BELVOIR VA 22060-6218

1   DIRECTOR
    US ARMY RSCH LABORATORY
    ATTN AMSRL CI AI R REC MGMT
    2800 POWDER MILL RD
    ADELPHI MD 20783-1197

1   DIRECTOR
    US ARMY RSCH LABORATORY
    ATTN AMSRL CI LL   TECH LIB
    2800 POWDER MILL RD
    ADELPHI MD 20783-1197

1   DIRECTOR
    US ARMY RSCH LABORATORY
    ATTN AMSRL D   D SMITH
    2800 POWDER MILL RD
    ADELPHI MD 20783-1197

2   CDR US ARMY TACOM-ARDEC
    ATTN AMSTA AR WEE A
            K KLINGAMAN N ELDREDGE
    B3124
    PICATINNY ARSENAL NJ 07806-5000

    ABERDEEN PROVING GROUND

2   DIRECTOR
    US ARMY RSCH LABORATORY
    ATTN AMSRL CI LP (TECH LIB)
    BLDG 305 APG AA

5   DIRECTOR
    US ARMY RSCH LABORATORY
    ATTN AMSRL WM B W OBERLE
    BLDG 4600

1   DIRECTOR
    US ARMY RSCH LABORATORY
    ATTN AMSRL WM BD B HOMAN
    BLDG 4600

INTENTIONALLY LEFT BLANK

REPORT DOCUMENTATION PAGE

Public reporting burden for this collection of information is estimated to average 1 hour per response, including the time for reviewing instructions, searching existing data sources, gathering and maintaining the data needed, and completing and reviewing the collection of information. Send comments regarding this burden estimate or any other aspect of this collection of information, including suggestions for reducing this burden, to Washington Headquarters Services, Directorate for Information Operations and Reports, 1215 Jefferson Davis Highway, Suite 1204, Arlington, VA 22202-4302, and to the Office of Management and Budget, Paperwork Reduction Project (0704-0188), Washington, DC 20503.

1. AGENCY USE ONLY (Leave blank)	2. REPORT DATE	3. REPORT TYPE AND DATES COVERED
	December 2001	Final

4. TITLE AND SUBTITLE

Dynamic Vivacity and Its Application to Conventional and Electrothermal-Chemical (ETC) Closed Chamber Results

5. FUNDING NUMBERS

PR: 62618AH75

6. AUTHOR(S)

Oberle, W.F. (ARL)

7. PERFORMING ORGANIZATION NAME(S) AND ADDRESS(ES)

U.S. Army Research Laboratory
Weapons & Materials Research Directorate
Aberdeen Proving Ground, MD 21005-5066

8. PERFORMING ORGANIZATION REPORT NUMBER

9. SPONSORING/MONITORING AGENCY NAME(S) AND ADDRESS(ES)

U.S. Army Research Laboratory
Weapons & Materials Research Directorate
Aberdeen Proving Ground, MD 21005-5066

10. SPONSORING/MONITORING AGENCY REPORT NUMBER

ARL-TR-2631

11. SUPPLEMENTARY NOTES

12a. DISTRIBUTION/AVAILABILITY STATEMENT

Approved for public release; distribution is unlimited.

12b. DISTRIBUTION CODE

13. ABSTRACT (Maximum 200 words)

Historically, dynamic vivacity has been used extensively in propellant lot acceptance. More recently, dynamic vivacity has been used in the analysis of closed chamber experimental data to assess propellant grain surface area behavior during combustion. The objective of this report is to (a) examine the physical meaning of dynamic vivacity; (b) theoretically explore the behavior of dynamic vivacity for conventionally ignited charges of various geometries, including layered propellant charges; and (c) determine the appropriate method for applying dynamic vivacity to electrothermal-chemical (ETC) closed chamber data. The results presented indicate that dynamic vivacity is a robust statistic for assessing grain surface area behavior during combustion as long as the burn rate exponent in Vielle's Law is between approximately 0.7 and 1.0. If the burn rate exponent is greater than 1.0, the nature of the propellant surface area deduced from the dynamic vivacity appears to be distorted. In these cases, the dynamic vivacity always indicates a progressive grain geometry. From the cases studied, it appears that grain fracture during combustion will not significantly change the dynamic vivacity results unless the original grain possess a progressive grain geometry and the fractured grain pieces are relatively large. Finally, it appears that ETC ignition does not impact the shape of the dynamic vivacity curve but only affects the magnitude of the curve.

14. SUBJECT TERMS

closed chamber   dynamic vivacity   vivacity
combustion   propellant

15. NUMBER OF PAGES

55

16. PRICE CODE

17. SECURITY CLASSIFICATION OF REPORT	18. SECURITY CLASSIFICATION OF THIS PAGE	19. SECURITY CLASSIFICATION OF ABSTRACT	20. LIMITATION OF ABSTRACT
Unclassified	Unclassified	Unclassified	